FACULTY OF TEXTILE ENGINEERING TUL

Advanced Fibrous Structures Based on Bacterial Cellulose

Sebnem Sözcü, M.Sc.

SUMMARY OF THE THESIS

Title of the thesis: **Advanced Fibrous Structures Based on Bacterial Cellulose**

Author: **Sebnem Sözcü, M. Sc.**

Field of study: **Textile Engineering**

Mode of study: **Full-time**

Department: **Department of Material Engineering**

Supervisor: **Ing. Blanka Tomková, Ph.D.**

Co-supervisor: **doc. Mohanapriya Venkataraman, M.Tech., M.F.Tech., Ph.D.**

Composition of the dissertation defense committee:

Chairman:	
doc. Ing. Jiří Chvojka, Ph.D.	FT TUL, Department of Nonwovens and Nanofibrous Materials
Vice-Chairman:	
doc. Ing. Veronika Tunáková, Ph.D.	FT TUL, Department of Material Engineering
prof. Ing. Petr Sáha, CSc., dr. h. c. (opponent)	Tomas Bata University in Zlín The Centre of Polymer Systems
doc. Dr. Ing. Dana Křemenáková	FT TUL, Department of Material Engineering
doc. Ing. Daniela Špánek Lubasová, Ph.D.	FT TUL, Department of Textile Evaluation
Ing. Jan Marek, CSc. (opponent)	INOTEX spol. s r.o.
Ing. Josef Večerník, CSc.	Večerník s.r.o.

The dissertation is available at the Dean's Office FT TUL.

Liberec 2026

Abstract

This thesis presents a sustainable and additive-free approach for producing bacterial cellulose (BC) aerogels and cryogels from *Acetobacter xylinum* under standardized cultivation using bio-based feedstocks, including fermentation by-products. Despite controlled conditions, inherent biological variability influences fibril formation and network architecture, introducing minor structural differences. The study systematically evaluates the effect of drying pathways and pre-freezing strategies on multiscale structure and functional performance (thermal, acoustic, mechanical) of BC materials. Three drying routes were applied: room-temperature drying, supercritical CO_2 ($ScCO_2$) drying after solvent exchange, and freeze-drying with controlled pre-freezing (–18 °C, liquid nitrogen at –196 °C, and in situ freezing). Additionally, mechanically disintegrated and regenerated BC was processed via lyophilization under identical conditions.

Drying pathway governs pore preservation and fibrillar organization, leading to distinct structure–property relationships. $ScCO_2$-dried aerogels exhibited the highest surface area (~124 m^2/g), pore volume (~0.35–0.36 cm^3/g), and uniform mesoporous structure (~9.77 nm), with ultralow density (~0.01 g/cm^3). Freeze-dried cryogels showed moderate surface area (~51.43 m^2/g) and mesoporosity (~10.6 nm), but achieved the lowest thermal conductivity (~0.030 $W \cdot m^{-1} \cdot K^{-1}$). Regenerated BC displayed reduced surface area (~31.1 m^2/g) and enlarged pores (~23.36 nm) due to fibril aggregation, resulting in the highest sound absorption coefficient (SAC ≈ 0.68).

Overall, ambient drying induced densification, $ScCO_2$ drying maximized structural uniformity and porosity, freeze-drying optimized thermal insulation, and regeneration enhanced acoustic performance. These results establish drying strategy and structural preservation as the primary parameters for tailoring additive-free BC materials toward application-specific thermal and acoustic functions.

Keywords: Bacterial Cellulose, *Acetobacter Xylinum* strain, morphology, surface unevenness, cyrogel, aerogel, lyophilization

Anotace

Cílem práce bylo vyvinout a charakterizovat udržitelný proces výroby bakteriálních celulózových (BC) aerogelů a kryogelů produkovaných baktériemi Acetobacter xylinum bez použití aditiv, za standardizovaných podmínek kultivace a s využitím bio surovin, včetně vedlejších produktů fermentace. Inherentní biologická variabilita zde ovlivňuje tvorbu fibril a architekturu celulózové sítě a způsobuje drobné strukturní rozdíly i přes kontrolované podmínky přípravy BC. Byl systematicky zkoumán vliv sušicích způsobů a strategií předmrazování na morfologickou strukturu a funkční charakteristiky (tepelné, akustické, mechanické) výsledné BC. Byly použity tři sušicí způsoby: sušení při pokojové teplotě, sušení v superkritickém CO_2 ($ScCO_2$) po náhradě rozpouštědla a lyofilizace s kontrolovaným předmrazováním (−18 °C, kapalný dusík při −196 °C a in − situ zmrazování). Mechanicky dezintegrovaná a regenerovaná BC byla navíc zpracována lyofilizací za stejných podmínek. Bylo prokázáno, že způsob sušení rozhoduje o zachování pórů a organizaci fibril, což vede také k morfologickým rozdílům a odlišnostech vlastností. Aerogely sušené $ScCO_2$ vykazovaly největší měrný povrch (~124 m^2/g), objem pórů (~0,35–0,36 cm^3/g) a stejnoměrnou mezoporézní strukturu (velikost pórů ~9,77 nm) s extrémně nízkou hustotou (~10 kg/m^3). Lyofilizované kryogely vykazovaly střední měrný povrch (~51,43 m^2/g) a mezoporozitu (velikost pórů ~10,6 nm), ale dosáhly nejnižší tepelné vodivosti (~0,030 $W \cdot m^{-1} \cdot K^{-1}$). Regenerovaný BC vykazoval zmenšený povrch (~31,1 m^2/g) a zvětšené póry (velikost pórů ~23,36 nm) v důsledku agregace fibril, což vedlo k nejvyššímu koeficientu zvukové pohltivosti (SAC ≈ 0,68). Sušení při pokojové teplotě vyvolalo kolaps struktury sítě (zhuštění), sušení $ScCO_2$ maximalizovalo strukturální stejnoměrnost a pórovitost, lyofilizace optimalizovala tepelnou izolaci a regenerace zlepšila akustickou pohltivost. Tyto výsledky umožnují výběr strategie sušení pro tvorbu vhodné struktury BC, která je primárním parametrem pro realizaci tepelných a akustických funkcí BC specifických pro dané aplikace.

Klíčová slova: bakteriální celulóza, kmen *Acetobacter xylinum*, morfologie, povrchová nerovnoměrnost, kryogel, aerogel, lyofilizace.

Summary

Contents

1. Introduction

The textile industry poses significant environmental challenges associated with both synthetic and natural fibers. Synthetic polymers contribute to greenhouse gas emissions and persistent microplastic pollution, while natural fibers, despite biodegradability, require high water, land, and chemical inputs, generating substantial environmental burdens [1–3]. These limitations highlight the need for sustainable material alternatives and resource-efficient production strategies.

Bio-based materials have emerged as promising candidates due to their renewability and environmental compatibility. Among them, cellulose is particularly important because of its abundance, mechanical strength, and versatility; however, plant-derived cellulose requires energy-intensive purification and chemical processing. Bacterial cellulose (BC) offers a more sustainable alternative, being biosynthesized in a highly pure form and exhibiting high crystallinity, mechanical robustness, and water-holding capacity suitable for advanced applications[4–9].

Aerogels further enhance material performance through ultralow density, high porosity, and large surface area, enabling effective thermal and acoustic insulation. However, conventional BC aerogel processing often relies on non-sustainable inputs, and the influence of drying pathways on structure–property relationships remains insufficiently clarified under controlled conditions [10–13].

This thesis develops an additive-free, sustainable approach for producing BC aerogels and cryogels from *Acetobacter xylinum* under standardized cultivation. The study systematically evaluates the effect of drying strategies—room-temperature drying, supercritical CO_2 drying, and freeze-drying with controlled pre-freezing—on multiscale structure and functional properties. Regenerated BC networks are also investigated within the same framework.

The thesis demonstrates that drying-induced stresses, freezing kinetics, and solvent exchange govern pore preservation and nanofibrillar organization, while intrinsic biological variability introduces minor structural differences. By directly comparing processing routes under identical conditions, the thesis establishes a consistent structure–property framework and provides a scalable pathway for tailoring additive-free BC materials for insulation, filtration, and related applications.

2. Research Gap, Aim, Motivation and Objectives of the Dissertation

Despite extensive research on bacterial cellulose (BC), consistent structure–property relationships remain insufficiently understood due to intrinsic biological variability and processing diversity. BC biosynthesis is governed by living microorganisms, and even under controlled conditions, minor variations in microbial activity and local growth environments affect fibril formation and network architecture, limiting comparability across studies. This challenge is compounded by the lack of systematic investigations linking drying pathways and pre-freezing conditions to

thermal and acoustic performance under identical conditions, while regenerated BC as an additive-free route remains underexplored. In addition, many reported methods rely on chemical additives or complex processing, reducing sustainability and scalability [14–16]. Although stabilization, freezing, and drying are known to influence porosity, density, and functional behavior, simplified and environmentally responsible processing strategies have not been evaluated within a unified framework.

Accordingly, this thesis develops and systematically assesses sustainable, additive-free processing routes for BC aerogels and cryogels under standardized cultivation. The thesis focuses on how drying strategies—room-temperature drying, freeze-drying with controlled pre-freezing, and supercritical CO_2 drying—govern pore preservation, nanofibrillar organization, and functional performance, while also evaluating regenerated BC as an alternative route. The objectives are to produce additive-free BC, analyze the effects of processing parameters on the structure and surface characteristics, quantitatively evaluate key functional properties, establish processing–structure–property relationships, and define a performance–sustainability framework identifying conditions where simplified methods achieve comparable outcomes. Overall, the thesis provides a consistent basis for understanding the combined influence of biological variability and processing on BC materials and supports scalable, environmentally responsible design strategies.

3. Overview of the current state of the art

3.1 Sustainable Approaches to Bacterial Cellulose Synthesis

Recent studies emphasize sustainable BC production using renewable and waste-derived substrates (e.g., fruit waste, molasses, lignocellulosic sources), enabling cost-effective and environmentally favorable biosynthesis. However, BC formation remains biologically regulated (*Komagataeibacter xylinus*), and even under controlled conditions, variability in microbial activity influences fibril assembly and network structure [17–20]. Process optimization (pH, temperature, oxygen) and bioreactor systems improve yield, yet many approaches still rely on chemical additives or modifications, limiting full sustainability [21–23]. Comparative studies show that low-density aerogels (4.2–22.8 kg/m³; $\lambda \approx 25.7$ mW/mK) can be achieved using additives [24], whereas waste-derived BC processed via $ScCO_2$ exhibits $\lambda \approx 13$ mW/(mK), demonstrating feasibility of additive-reduced routes[25].

3.2 Influence of Drying Methods on Bacterial Cellulose Pellicles

Drying governs BC structure and performance. Conventional drying induces pore collapse and densification, reducing porosity and surface area [26]. Freeze-drying and $ScCO_2$ drying preserve the nanofibrillar network: freeze-drying relies on ice templating, while $ScCO_2$ drying minimizes capillary stress through solvent exchange,

producing low-density, highly porous aerogels. Comparative studies indicate higher surface area and porosity for $ScCO_2$-dried materials, whereas freeze-dried structures show variability of properties depending on freezing conditions [27,27–30]. Systematic comparisons under consistent conditions remain limited.

3.3 Effect of Freezing Conditions for Freeze-Drying

Pre-freezing determines pore morphology. Rapid LN freezing produces uniform, interconnected networks (fibrils ~10–100 nm), while slower freezing leads to larger ice crystals, reduced porosity, and structural heterogeneity [28]. Although LN freezing improves pore preservation, surface cracking may occur. Overall, freeze-drying and $ScCO_2$ drying outperform thermal drying, which promotes fiber aggregation and dense structures. LN-assisted freezing reduces structural collapse compared to conventional methods, though variability persists. SEM consistently confirms interconnected nanofibrillar networks as the basis of BC functionality [31–34].

3.4 Functional Properties and Application Constraints

BC aerogels are hydrophilic (contact angle ~30°), and moisture exposure can induce swelling and structural degradation [35]. While high porosity supports biomedical and absorption applications, it may limit filtration and textile performance [36]. Thermal properties are structure-dependent; increased porosity via freeze-drying reduces thermal conductivity, while controlled freezing enables further tuning of heat transfer behavior [8,37] .

3.5 Comparative Assessment of Freeze-Drying and $ScCO_2$ Drying

Freeze-drying and $ScCO_2$ drying both preserve BC nanostructure but differ in mechanism and outcomes. Freeze-drying is accessible but strongly dependent on freezing conditions, leading to structural variability. In contrast, $ScCO_2$ drying eliminates surface tension effects, producing more uniform, low-shrinkage aerogels with higher surface area and structural fidelity [16,38]. Despite extensive studies, systematic comparisons of freezing regimes with $ScCO_2$ drying under additive-free, standardized conditions remain lacking, highlighting the need to define sustainable and scalable BC processing pathways.

4. Experimental Parts

4.1Materials

Acetobacter xylinum (CCM 2360, Czech Collection of Microorganisms, Brno) was used for bacterial cellulose production. Crystal white sugar (TTD, Czech Republic) and black tea (PG Tips) served as carbon and nitrogen sources, respectively. Anhydrous Na_2CO_3 (Chemapol, Prague) was applied for purification, while polyester

nonwoven (PES NW, 10 and 20 GSM; JX Nippon ANCI) was used as a support material where required [39].

Liquid nitrogen (LovoChemie, Prague) enabled rapid pre-freezing, and acetone (ACS grade, Merck) was used for solvent exchange in $ScCO_2$ drying [30].

Crystalline graphite PMM 7 (ECOLUBE, <7 µm) was introduced as a conductive filler to enhance thermal stability and electrical conductivity. All experiments were performed using deionized water.

4.2 Preparation and Cultivation of Bacterial Cellulose

Bacterial cellulose (BC) was synthesized in a sweetened black tea medium containing 48% (w/v) sugar and 1.2% (w/v) tea, boiled for 20 min and cooled prior to inoculation. *Acetobacter xylinum* concentration was adjusted using a McFarland densitometer, and 10% (v/v)[1] inoculum was introduced into the medium. Static cultivation was performed at 24 ± 3 °C with initial pH ~5 (decreasing to ~4), producing pellicles (~3 mm) after 96 h and up to ~5 mm after 240 h. The overall process from cultivation to drying ($ScCO_2$, lyophilization) is illustrated in Figure 4.1, while regeneration via mechanical disintegration and freeze-drying is shown in Figure 4.2.

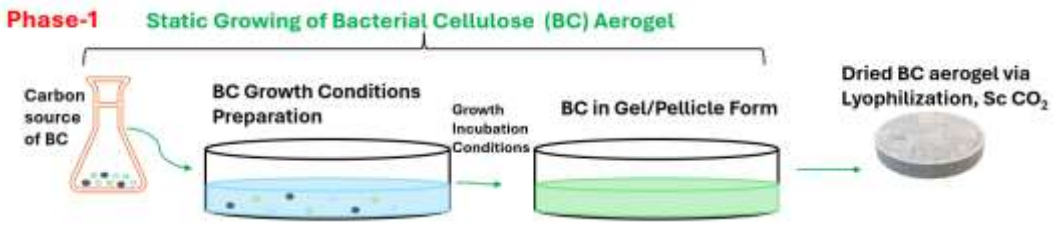

Figure 4.1 Illustration of static growing of bacterial cellulose (BC) aerogel.

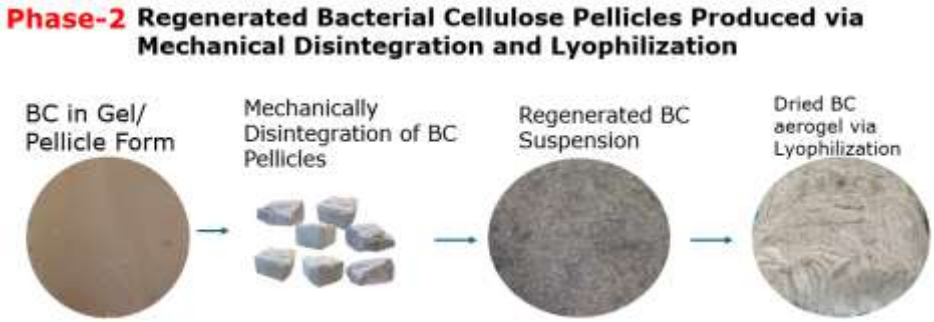

Figure 4.2 Illustration of regenerated bacterial cellulose pellicles produced via mechanical disintegration and lyophilization.

Regenerated BC aerogels were obtained by disintegrating pellicles into a fibrillated suspension followed by lyophilization, with conditions summarized in Table 4.1. For

[1] Weight/volume (% w/v) represents grams of solute per 100 mL of solution, while volume/volume (% v/v) represents millilitres of solute per 100 mL of solution.

investigation of composite preparation, crystalline graphite (PMM 7) was dispersed into the regenerated BC suspension prior to freezing, enabling its incorporation within the fibrillar network during subsequent freeze-drying.

Table 4.1 Cultivation parameters and experimental conditions applied for BC film formation [39].

Experimental Conditions	*Acetobacter xylinum* Cultivation Parameters
Cell concentration (inoculum)	1.3×10^9 cells/mL (by McFarland device)
Culture method	Static Culture
Growing temperature	24 ± 3 °C
Initial pH (tea medium for growing bacteria)	5 (pH indicator paper)
Final pH of bacteria medium	4 (pH indicator paper)
Duration of experiment	240 hours

4.3 Sample Preparation

The experimental work was conducted in two stages. First, BC pellicles were produced via static cultivation, purified, and dried with form stabilization using polyester nonwoven (PES NW) fabrics (MILIFE 10 and 20). In the second stage, identically prepared pellicles were dried without support to evaluate the influence of different drying methods. The properties of PES fabrics are summarized in Table 4.2.

Table 4.2 Properties of used polyester non-woven fabric (MILIFE) [40,41].

Materials	Structure	GSM (g/m^2)	Thickness (mm)	Air Permeability (mm/s)
Milife 10	Two-directional PES filaments fabricated via thermal bonding	10	0.068 ± 0.002	6827.5
Milife 20		20	0.070 ± 0.002	4035

4.3.1 BC Film Growth and Form Stabilization

BC pellicles were obtained via static cultivation of *Acetobacter xylinum* in Petri dishes and larger containers, forming layers (~2–3 mm) at the air–liquid interface. Drying without support caused shrinkage, wrinkling, and localized collapse due to capillary stresses and uncontrolled ice crystal formation during freezing, leading to heterogeneous pore structures. To mitigate these effects, porous PES nonwoven fabrics were introduced to provide mechanical stabilization, improve thickness uniformity, and promote homogeneous heat and mass transfer during freezing and

drying. Multiple stabilization configurations were evaluated (Table 4.3). Minor thickness and structural variations persisted due to the biologically regulated nature of BC synthesis, influencing fibril organization and drying response.

Figure 4.3 Synthesis of BC samples under static cultivation conditions. (a) Growth of BC pellicles in a Petri dish; (b) magnified view of BC pellicles with thickness of approximately 2–3 mm; (c) rectangular plastic container for large-area sample cultivation.

Table 4.3 Experimental conditions of all BC samples.

Sample Name	Description	Thickness (cm)	Drying Method	Pre-freezing Condition
RT-BC	Room-temperature dried BC pellicle; no supportive material used	0.016	Room Temperature	Non-applicable (N/A)
Lyo-BC-NW20-1	BC film placed between NW (MILIFE 20) fabrics	0.45	Lyophilization	Conventional freezing at -18 °C for 24 h
Lyo-BC-NW10-Bot	Bottom of the Petri dish placed on NW fabric (MILIFE 10), and BC film placed on it	0.52		
Lyo-BC-NW10-Top	Top of the Petri dish covered with NW fabric (MILIFE 10), and BC film placed on it	0.56		
Lyo-BC-NW20-Bot	Bottom of the Petri dish placed on NW fabric (MILIFE 20), and BC film placed on it	0.5		
Lyo-BC-Frame-1	BC film placed in plastic frame structure	0.52		
Lyo-BC-LN1	Liquid nitrogen pre-freezing prior to lyophilization	0.72		
Lyo-BC-LN2		0.49		
Lyo-BC-LN3		0.27		
Sc-BC-NS-1		0.55	Sc CO_2	N/A

Sc-BC-NS-2	No supportive (NS) material used	0.78		
Lyo-BC-NS-1		0.13	Lyophilization	Controlled shelf freezing (3 h) in Situ Freezing
Lyo-BC-NS-2		0.57		
Lyo-BC-NS-3		0.67		
Lyo-RBC-CS	Regenerated Bacterial Cellulose (BC)	0.58		
Ref-RBC	Reference for Regenerated BC sample	-		
RBC-Graphite	BC incorporated with crystalline graphite	-		

4.3.2 Room Temperature Drying Method

Room-temperature drying (24 ± 3 °C) removed water via slow evaporation, where capillary forces induced pore collapse, producing densified structures with reduced porosity. Although simple and low-energy, this method results in significant shrinkage and loss of the native porous network.

4.3.3 Freezing and Lyophilization

BC films were pre-frozen using conventional freezing (−18 °C, 24 h) or rapid LN freezing (−196 °C). Conventional freezing led to structural degradation due to uncontrolled ice crystal growth, whereas LN freezing limited crystal size and improved pore preservation. Subsequent lyophilization (−30 °C pre-freezing, −40 °C drying, 48 h, 0.133 mbar) enabled sublimation-driven drying with maintained structural integrity.

4.3.4 Drying Method without Fabric Support

To isolate drying effects, BC pellicles were processed without stabilization. $ScCO_2$ drying (Sc-BC-NS) and direct lyophilization (Lyo-BC-NS) were compared under identical conditions, enabling direct evaluation of drying-induced structural differences.

4.3.4.1 Lyophilization (In situ Freezing)

In situ freezing (−30 °C, 3 h) followed by drying at −33 °C (48 h, 36 Pa, Leosmak LEO-004 freeze dryer) with mild heating (25–30 °C) provided a continuous process without separate freezing. Prolonged freezing was avoided due to pore blockage and surface crystallization effects.

4.3.4.2 Supercritical CO_2 Drying

Water was replaced by acetone through stepwise solvent exchange, followed by drying at 65 °C and 90 bar for 48 h. This capillary-free process preserved the nanofibrillar structure with minimal shrinkage and high reproducibility [42].

Freezing conditions controlled ice-templated pore formation (LN → fine, uniform pores; conventional → heterogeneous pores), while drying pathways governed

structural preservation (lyophilization → sublimation-based; $ScCO_2$ → capillary-free), collectively determining porosity, uniformity, and reproducibility.

4.4 Tests and Methods

4.4.1 Morphological and Chemical Characterization

Microstructure was analyzed by SEM (Zeiss Ultra Plus, 2 kV) after Au/Pd coating, with elemental composition determined by EDX. Chemical structure was evaluated using ATR-FTIR (400–4000 cm^{-1}), enabling identification of functional groups.

4.4.2 Surface Roughness Analysis

Surface topography was assessed by confocal laser microscopy (Olympus LEXT OLS3100, 405 nm, 20×) following ČSN EN ISO 21920-2. Roughness (Rz) was calculated as[43,44]:

$$R_Z = R_P + R_V \tag{4.1}$$

Statistical evaluation was performed using ANOVA with Tukey post-hoc testing.

4.4.3 Water Contact Angle Measurements

Wettability was determined by WCA using a droplet shape analyzer with 0.05 mL deionized water, providing quantitative hydrophilicity assessment.

4.4.4 Compressibility and Load-Bearing Characteristics

Mechanical response was evaluated via compression testing (TIRA 2300, 50 N load cell) under force-controlled loading (up to 40 N), analyzing force–deformation behavior, pore collapse, and structural integrity.

4.4.5 Geometrical Analysis and Water Content Determination

Bulk density and porosity were calculated from mass and geometry using:

$$V_a\,[m^3] = hA \tag{4.2}$$

$$V_c[m^3] = M/\rho \tag{4.3}$$

$$P = 100(1 - V_c/V_a) \tag{4.4}$$

Water content was determined gravimetrically from wet–dry mass difference: $\frac{W_{wet}-W_{dry}}{W_{dry}}\ x\ 100$.

4.4.6 Specific Surface Area and Pore Volume Analysis

Textural properties were obtained via N_2 adsorption (77 K, Autosorb 6100). BET surface area (p/p_o = 0.05–0.30), total pore volume, and pore size distribution (DFT) were determined after degassing (50 °C, 48 h).

4.4.7 Thermal Analysis

Thermal behavior was analyzed by DSC (−50 to 500 °C, 10 °C/min). Thermal conductivity and diffusivity were measured using Alambeta under a 32 °C gradient [39]. Environmental conditions were monitored using iButton sensors (temperature and RH, 60 s intervals), with averaged values ensuring measurement stability [45,46].

4.4.8 Acoustic Absorption Measurements

Sound absorption was measured using a two-microphone impedance tube (100–5000 Hz, 40 mm thickness) based on the transfer function method [47,48]. Measurement limits were defined by tube geometry. Minor variability in acoustic response may arise from intrinsic biological differences in BC structure despite standardized processing.

5. Results and Discussion

5.1 Effect of Room Temperature Drying Method on BC Pellicles

5.1.1 Morphological and Elemental Characterization of Room-Temperature Dried Bacterial Cellulose (BC)

Figure 5.1 shows that room-temperature drying produces a dense, compact nanofibrillar network due to capillary-induced pore collapse during slow evaporation, while maintaining overall structural continuity. Localized agglomerates indicate possible residual impurities.

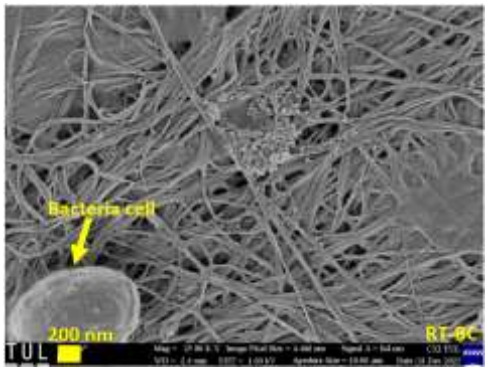

Figure 5.1 SEM image of bacterial cellulose dried at room temperature.

EDX analysis (Figure 5.2) confirms cellulose composition with dominant carbon (81.7 wt%) and oxygen (17.7 wt%), and minor traces of Ca, Na, and Mg attributed to residual impurities; Au peaks arise from coating.

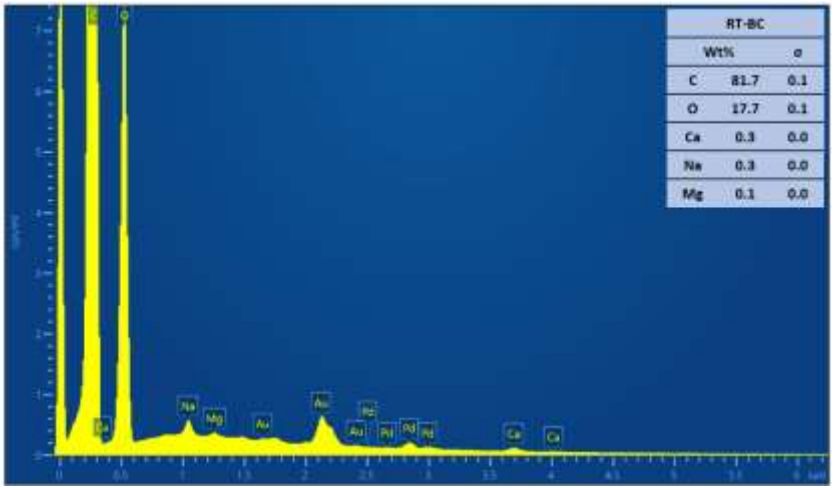

Figure 5.2 EDX spectrum of room temperature dried bacterial cellulose sample.

Overall, room-temperature drying induces structural densification without altering the elemental composition of BC.

5.1.2 Chemical Structure and Functional Group Characterization of Room-Temperature Dried Bacterial Cellulose

Figure 5.3 shows characteristic cellulose bands: O–H stretching (3200–3500 cm^{-1}), C–H stretching (~2900 cm^{-1}), and absorbed water (~1640 cm^{-1}). Peaks at 1000–1150 cm^{-1} and ~900 cm^{-1} confirm β-1,4-glycosidic linkages of cellulose I. Ambient drying preserves the chemical structure, while the pronounced O–H band reflects enhanced hydrogen bonding associated with structural densification.

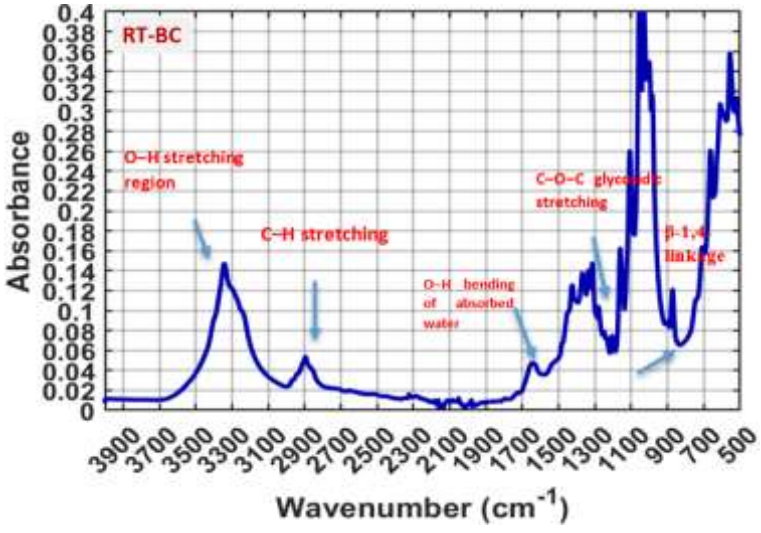

Figure 5.3 FTIR spectrum of bacterial cellulose dried at room temperature.

5.1.3 Density and Porosity Analysis of Room-Temperature Dried Bacterial Cellulose

Room-temperature drying yielded an apparent volume of 8.23 cm^3 and cellulose volume of 3.35 cm^3, resulting in porosity of 59.4%. Increased density indicates

capillary-driven compaction and partial pore collapse, consistent with SEM observations, while measurable porosity is retained due to the interconnected nanofibrillar network. FTIR confirms unchanged chemical structure. Minor variations may arise from intrinsic biological variability during BC synthesis.

5.2 Effect of Super Critical Drying on Bacterial Cellulose Pellicles

This section compares supercritical CO_2 drying and freeze-drying applied to unsupported, additive-free BC to isolate drying effects on the nanofibrillar structure.

5.2.1 Surface Morphology and Microstructural Characterization of BC

Figure 5.4 shows that $ScCO_2$-dried BC aerogels (Sc-BC-NS-1, Sc-BC-NS-2) exhibit a highly porous, interconnected nanofibrillar network with minimal collapse across multiple scales (10 µm–200 nm). Capillary stress elimination via acetone solvent exchange preserves the native 3D structure.

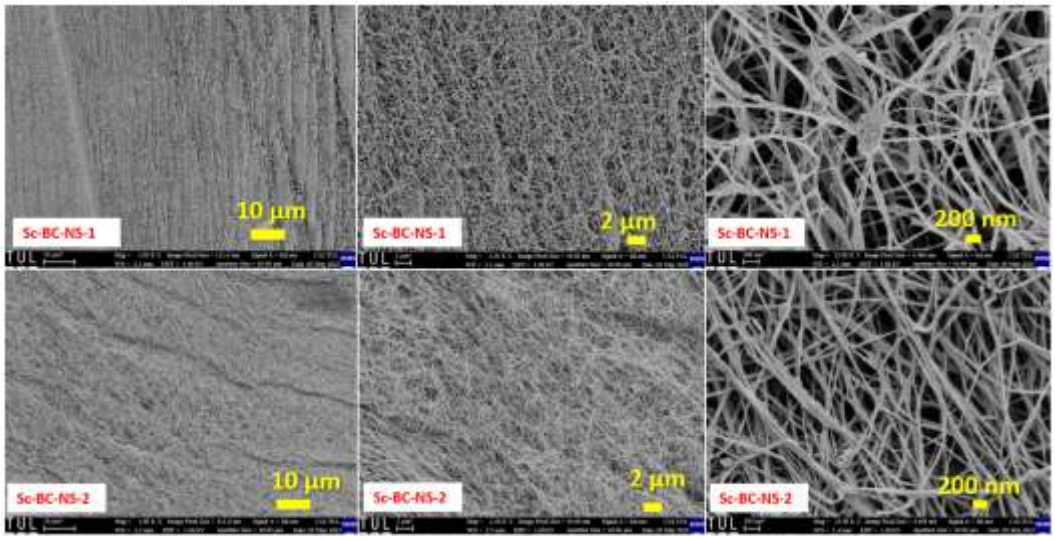

Figure 5.4 SEM images comparing BC aerogels in different magnification.

Fibril diameters were ~55.58 nm (Sc-BC-NS-1) and ~46.12 nm (Sc-BC-NS-2) (Figure 5.5), forming a uniform network consistent with high surface area (~124.02 m^2/g) and pore volume (~0.36 cm^3/g), confirming effective mesostructured preservation.

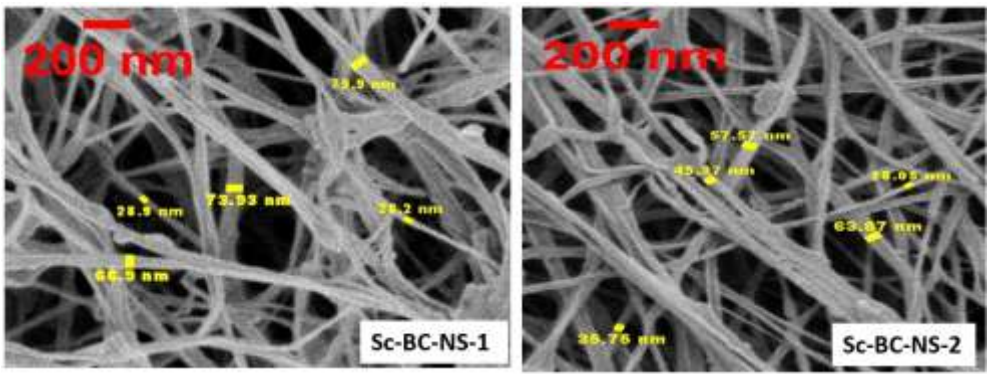

Figure 5.5 Diameter of fibrils in BC Aerogels.

5.2.2 Elemental Composition Analysis of Bacterial Cellulose

EDX (Figure 5.6) confirms high-purity cellulose with dominant C (52.3 wt%) and O (47.5 wt%) and trace impurities, indicating preserved polymer composition and structural integrity after $ScCO_2$ drying.

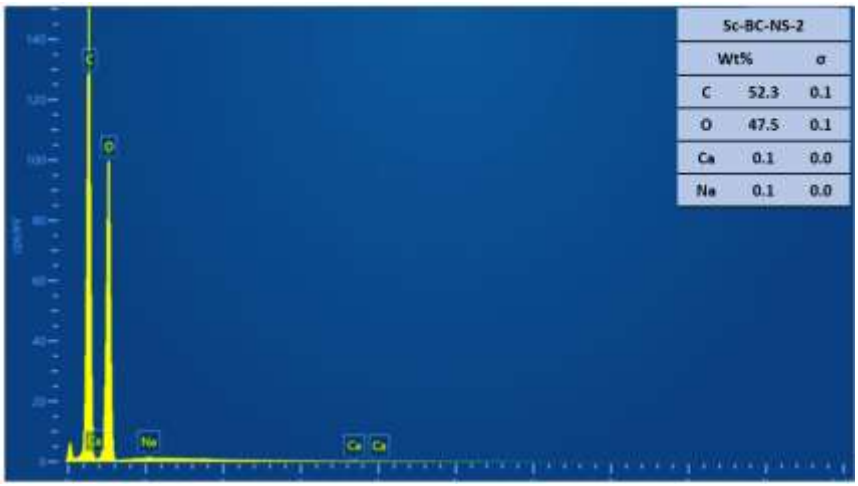

Figure 5.6 EDX finding for Sc-BC-NS-2 bacterial cellulose aerogels.

5.2.3 Geometrical Analysis

Table 5.1 shows that wet BC (>99% water, ~0.8 cm thickness, ~90.2 g) is transformed into ultralight aerogels (~0.01 g/cm³, ~99.1% porosity) with limited shrinkage (~18–19%), confirming effective structural preservation through solvent exchange and controlled $ScCO_2$ drying.

Table 5.1 Geometrical Analysis of BC samples dried with Sc CO_2.

Sample No	Drying Method	Before Drying			After Drying					
		Wet Thickness (cm)	Wet Mass (g)	Sample size (cm)	Dry Thickness (cm)	Dry Mass (g)	Apparent Volume (cm^3)	Volume of Cellulose (cm^3)	Porosity (%)	S
Sc-BC-NS-1	Sc CO_2	0.68	76.56	9x9	0.55	0.61	44.69	0.39	99.12	8
Sc-BC-NS-2		0.95	103.83	9.5x9.5	0.78	0.87	67.81	0.56	99.17	9

5.2.4 Functional Group and Chemical Structure Analysis of Bacterial Cellulose

FTIR spectra of Sc-BC-NS-1 and Sc-BC-NS-2 (Figure 5.7) show characteristic cellulose I bands, confirming preserved chemical structure after $ScCO_2$ drying. Key peaks include O–H stretching (~3340 cm^{-1}), C–H stretching (~2890 cm^{-1}), adsorbed water (~1640 cm^{-1}), and C–O/C–O–C vibrations (1160–1030 cm^{-1}) with β-glycosidic

linkage (~895 cm^{-1}). Similar spectra indicate consistent hydrogen-bonding and chemical stability.

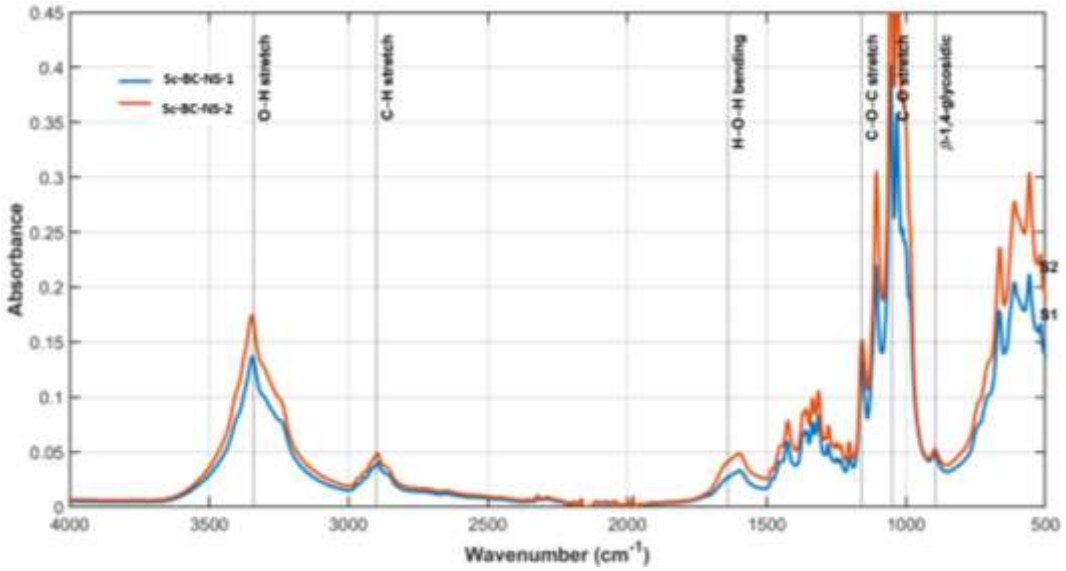

Figure 5.7 FT-IR analysis of bacterial cellulose aerogels.

5.2.5 3D Surface Roughness and Topography Analysis of Bacterial Cellulose

CLSM analysis (Figure 5.8) shows continuous aerogel surfaces with distinct roughness differences: Sc-BC-NS-1 (Rz = 58.04 µm) is rougher than Sc-BC-NS-2 (Rz = 21.49 µm).

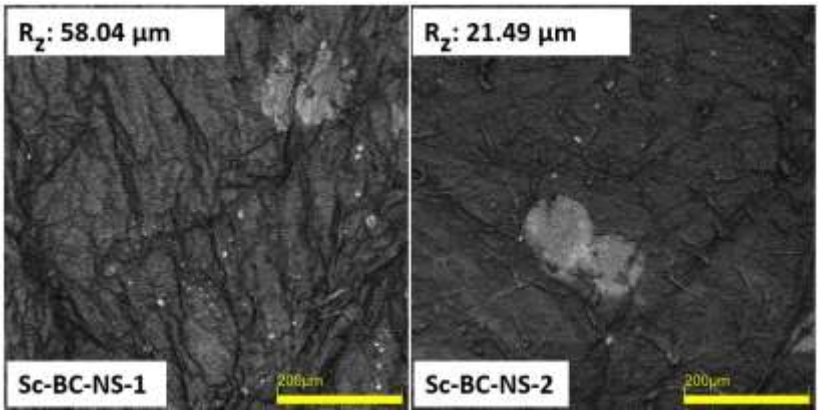

Figure 5.8 Analysis of surface roughness of aerogels. Objective: 20× for all photos. The scale bar indicates 200 µm. Rz: average roughness depth.

3D topography (Figure 5.9) confirms larger height variation in Sc-BC-NS-1 (−95 to +74 µm) compared to the more uniform Sc-BC-NS-2 (−41 to +40 µm), indicating differences in structural preservation.

Variations are attributed to pre-drying conditions and inherent biological variability affecting fibril organization despite identical drying parameters.

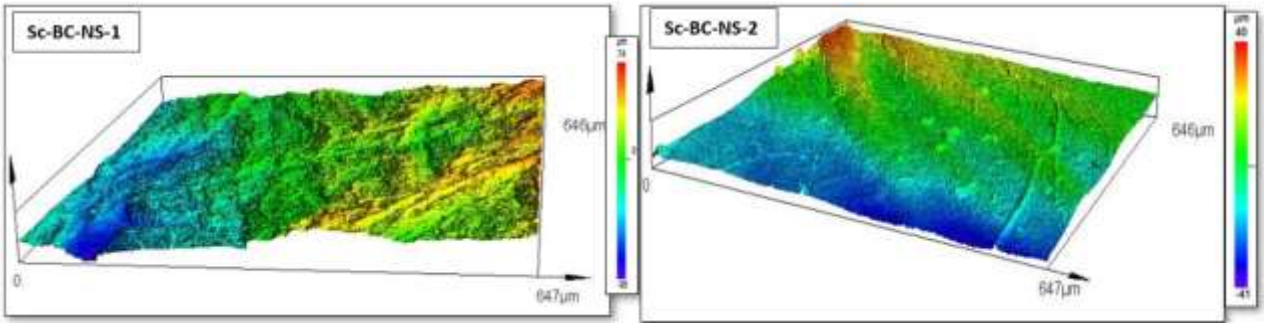

Figure 5.9 Three-dimensional surface topography of BC samples.

5.2.6 Specific Surface Area and Porosity Characterization of Bacterial Cellulose

BET analysis (Table 5.2) shows highly reproducible mesoporous structures for $ScCO_2$-dried BC aerogels, with surface areas of 124.02 and 122.93 m^2/g, pore volumes of 0.36 and 0.35 cm^3/g, and average pore diameter ~9.77 nm. Low standard deviations confirm structural uniformity, attributed to effective acetone solvent exchange and capillary-free drying. These values align with reported ranges (100–200 m^2/g; 0.3–0.4 cm^3/g) [30,31,49], noting possible underestimation of macroporosity by N_2 sorption.

Table 5.2 BET measurements of BC aerogels.

Sample	Drying Method	BET Surface Area (m^2/g)	Total Pore Volume (cm^3/g)	Average Pore Diameter (nm)
Sc-BC-NS-1	Supercritical CO_2	124.02	0.36	9.771
Sc-BC-NS-2		122.93	0.35	9.772
Mean		123.47	0.36	9.7715
Standard Deviation		0.77	0.007	0.00071

N_2 isotherms (Figure 5.10) exhibit Type IV with H3 hysteresis, indicating slit-like mesopores and negligible microporosity, with capillary condensation at $p/p_o \approx 0.8–0.9$ [32]. Sc-BC-NS-1 shows slightly higher uptake than Sc-BC-NS-2, confirming comparable mesoporosity.

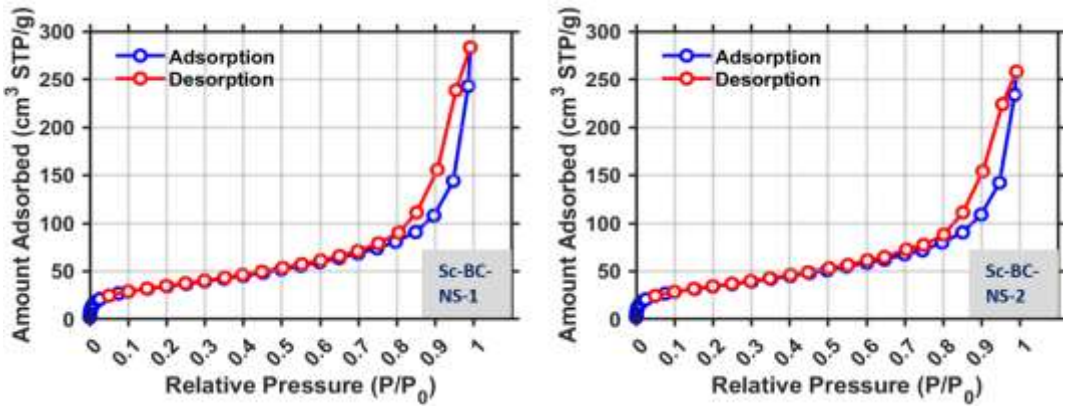

Figure 5.10 N_2 adsorption-desorption isotherms of the BC samples.

Overall, $ScCO_2$ drying preserves an open mesoporous network with high surface accessibility and minimal shrinkage.

5.2.7 Thermal Transition and Heat Flow Analysis of Bacterial Cellulose

Despite thickness differences (0.5 and 0.8 cm), Sc-BC-NS-1 and Sc-BC-NS-2 exhibit nearly identical BET properties and overlapping DSC curves (Figure 5.11), indicating uniform pore structure and consistent thermal behavior independent of geometry.

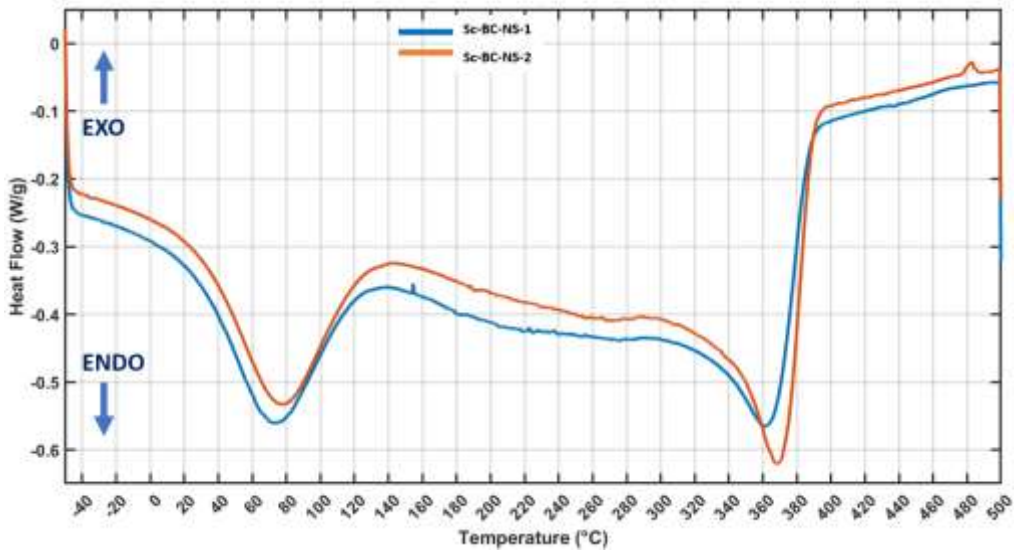

Figure 5.11 DSC results of aerogel samples.

Thermal transitions are governed by intrinsic aerogel structure, confirming homogeneous pore preservation through $ScCO_2$ drying.

5.2.8 Thermal Conductivity and Thermal Resistance of Bacterial Cellulose

$ScCO_2$-dried aerogels exhibit low thermal conductivity (0.040–0.042 $W \cdot m^{-1} \cdot K^{-1}$) and decreasing diffusivity with thickness (8.31 → 6.95 $mm^2 \cdot s^{-1}$), indicating effective insulation and slower heat propagation in thicker structures (Figure 5.12). Minor differences reflect variations in pore connectivity and fibril packing. The preserved open nanofibrillar network supports both thermal insulation and acoustic damping through enhanced airflow resistance and energy dissipation.

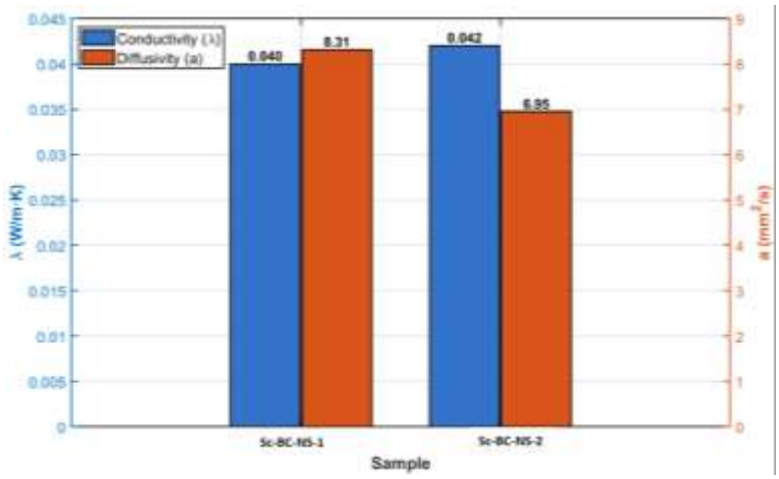

Figure 5.12 Thermal conductivity and diffusivity of Sc CO2 dried samples.

5.2.9 Monitoring of Environmental Conditioning Parameters (Temperature and Relative Humidity)

Environmental conditions remained stable (27.0–27.7 °C; 32–34 % RH) with low deviations, indicating minimal external influence during characterization (Figure 5.13). Minor variability may arise from localized surface conditions and intrinsic biological differences in BC structure.

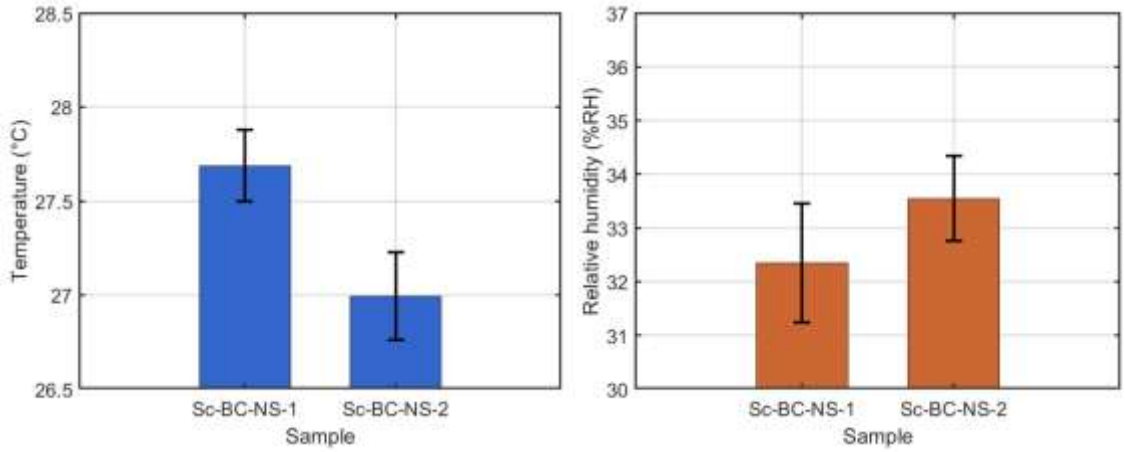

Figure 5.13 Thermal and humidity distribution of aerogel samples (left: temperature fluctuation; right: humidity fluctuation image).

5.2.10 Frequency-Dependent Sound Absorption Coefficient of Bacterial Cellulose

Aerogels show low absorption at low frequencies (SAC ≈ 0.039–0.047 at 1000 Hz) with oscillations due to measurement limits. Absorption increases with frequency and thickness, reaching 0.162 (Sc-BC-NS-1) and 0.281 (Sc-BC-NS-2) at 4000 Hz. At 5000 Hz, Sc-BC-NS-2 retains absorption (0.197), while Sc-BC-NS-1 is affected by measurement constraints.

Table 5.3 Band-averaged SAC values for aerogel samples.

Sample	Center Frequency (Hz)	Band (Hz)	SAC	Thickness (cm)
Sc-BC-NS-1	1000	891-1122	0.039	0.55
	4000	3548-4466	0.162	
	5000	4466-5623	0.000	
Sc-BC-NS-2	1000	891-1122	0.047	0.78
	4000	3548-4466	0.281	
	5000	4466-5623	0.197	

Overall, $ScCO_2$ aerogels exhibit low-to-moderate acoustic performance, improving with frequency and thickness, while maintaining high structural preservation.

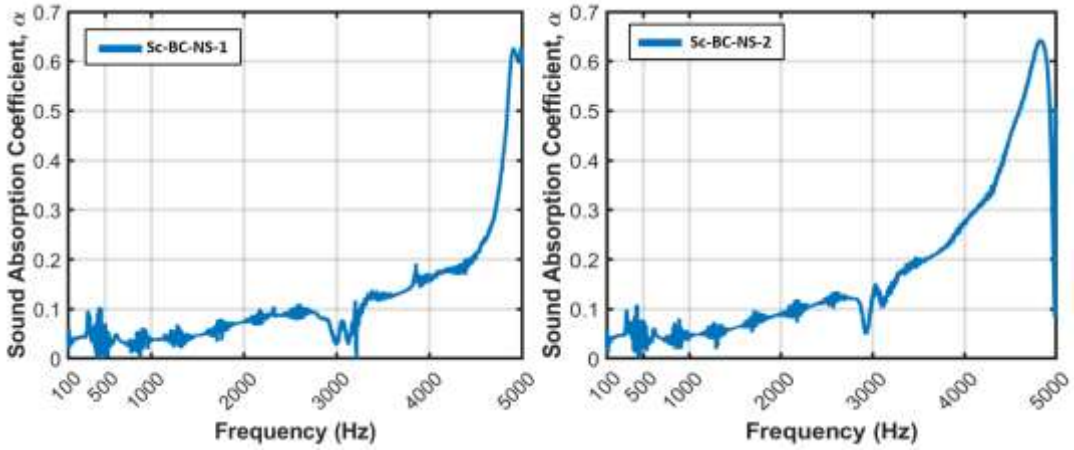

Figure 5.14 Frequency range spectrum of sound absorption coefficient of aerogel samples.

5.3 Impact of Different Pre-Freezing Conditions on Bacterial Cellulose Pellicles Prior to Lyophilization

5.3.1 Conventional pre-freezing at −18 °C: reference method

5.3.1.1 Surface Morphology and Microstructure Analysis of Bacterial Cellulose

SEM analysis (Figures 5.15–5.16) shows that conventional freezing (−18 °C) produces slow cooling, allowing ice crystal growth that templates larger, heterogeneous pores after sublimation. This leads to partial fibril aggregation and reduced nanofibrillar uniformity. Increased sample thickness (≈0.52 → 0.56 cm) further enhances ice crystal growth, resulting in stronger fiber bundling and larger macroporous domains. Overall, pore structure is governed by ice templating, where slow freezing promotes coarser porosity and partial densification.

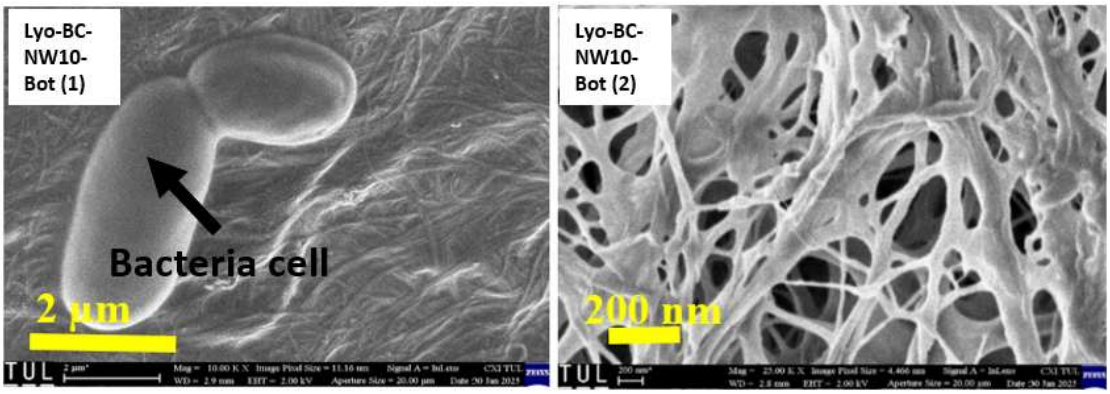

Figure 5.15 Surface (Lyo-BC-NW10-Bot -1) and cross-sectional (Lyo-BC-NW10-Bot -2) of BCAs pre-freezing via coventional method.

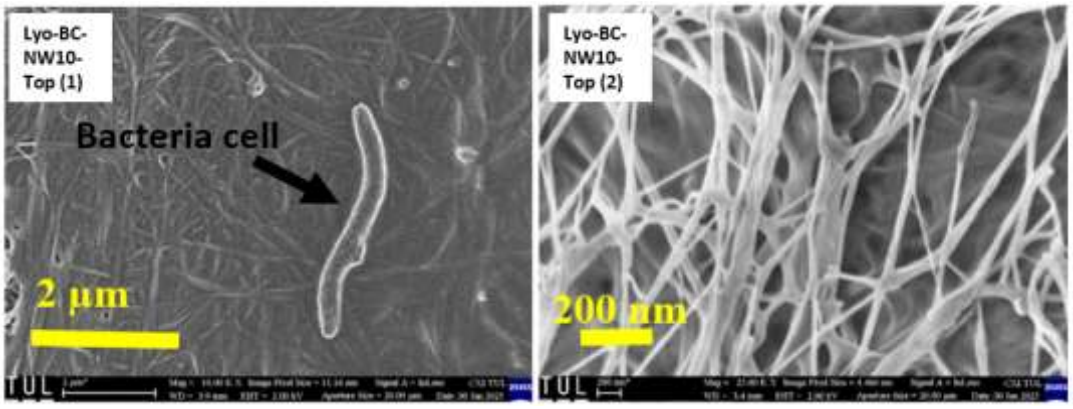

Figure 5.16 Surface (Lyo-BC-NW10-Top -1) and cross-sectional (Lyo-BC-NW10-Top -2) of BCAs pre-freezing via conventional method.

5.3.1.2 Elemental Composition Analysis of Bacterial Cellulose

EDX analysis (Figure 5.17) shows dominant carbon (57.1 wt%) and oxygen (42.6 wt%) with minor calcium (~0.3 wt%), confirming cellulose composition. Freezing and lyophilization affect morphology without altering chemical composition.

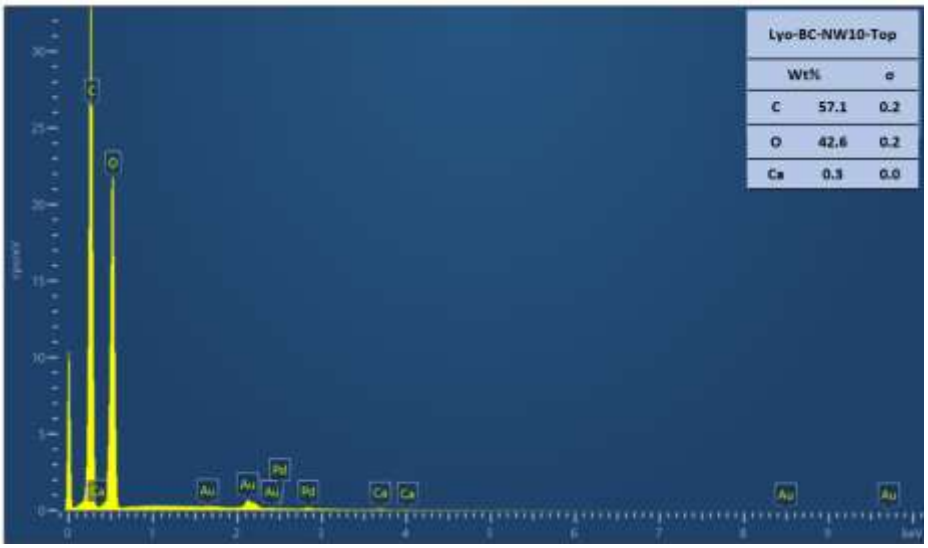

Figure 5.17 EDX Result of Lyo-BC-NW10-Top sample pre-frozen using the conventional method.

5.3.1.3 Geometrical Characterization of Bacterial Cellulose

Geometrical analysis (Table 5.4) shows very high porosity (98.81–99.87%) across all samples, confirming aerogel formation. Fabric-supported samples limit expansion and maintain stability (≈0.45 cm, ~98.8%), while Petri-dish configurations show similar thickness (0.50–0.56 cm) with slight variability due to boundary effects. Frame-supported samples achieve the highest porosity (99.87%), indicating strong influence of external constraints on shrinkage and pore development. Overall, geometry and support conditions significantly affect pore structure and fibril organization during conventional freezing.

Table 5.4 Geometrical analysis of Conventional pre-freezing used BC samples dried with lyophilization.

Samples	Description	Dry Thickness (cm)	Dry Mass (g)	Apparent Volume (cm^3)	Volume of Cellulose (cm^3)	Porosity (%)	Sample size (cm)	Shape
Lyo-BC-NW20-1	BC film placed between NW (MILIFE 20) fabrics	0.45	0.592	31.90	0.38	98.81	9.5	Circular (Diameter)
Lyo-BC-NW10-Bot	Bottom of the Petri dish placed on NW fabric (MILIFE 10), and BC film placed on it	0.52	0.99	61.39	0.63	98.97	12.26	Circular (Diameter)
Lyo-BC-NW10-Top	Top of the Petri dish covered with NW fabric (MILIFE 10), and BC film placed on it	0.56	0.35	48.49	0.22	99.54	10.5	Circular (Diameter)
Lyo-BC-NW20-Bot	Bottom of the Petri dish placed on NW fabric (MILIFE	0.50	0.39	34.70	0.25	99.28	9.4	Circular (Diameter)

	20), and BC film placed on it							
Lyo-BC-Frame-1	BC film placed in plastic frame structure	0.52	0.708	360.36	0.45	99.87	21x33	Rectangular

5.3.1.4 Compression Test

Compression tests (Figure 5.18) show nonlinear force–deformation behavior typical of highly porous BC aerogels. At low loads (<1 N), large strains (~5–10%) arise from elastic fibril bending and pore deformation. With increasing load (>2 N), progressive pore collapse leads to strain hardening, reaching ~28–30% strain at ~5 N without a plateau, indicating continuous densification. Stacked samples (n = 4) ensured stability; behavior remains characteristic of nanofibrillar aerogels.

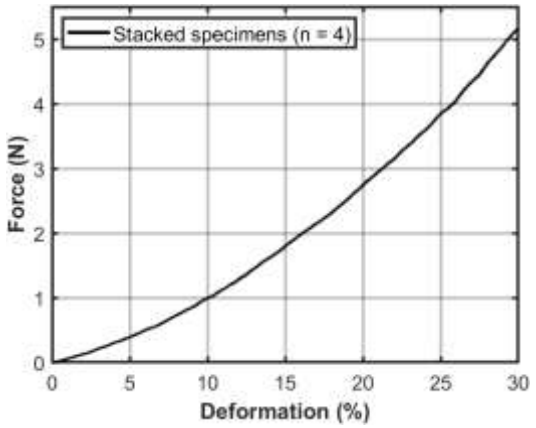

Figure 5.18 Force-deformation curve of stacked lyophilized bacterial cellulose aerogel specimens (n = 4).

5.3.1.5 3D Surface Roughness and Topography Analysis of Bacterial Cellulose

Confocal analysis (Figure 5.19) shows high surface heterogeneity, with Rz values of 331.47 µm (Lyo-BC-NW10-Bot), 131.25 µm (Lyo-BC-NW20-1), and 80.33 µm (Lyo-BC-NW10-Top). Higher roughness corresponds to heterogeneous pore structure and localized densification, while smoother surfaces indicate more uniform porosity. Surface roughness influences mechanical response by promoting localized deformation and gradual densification.

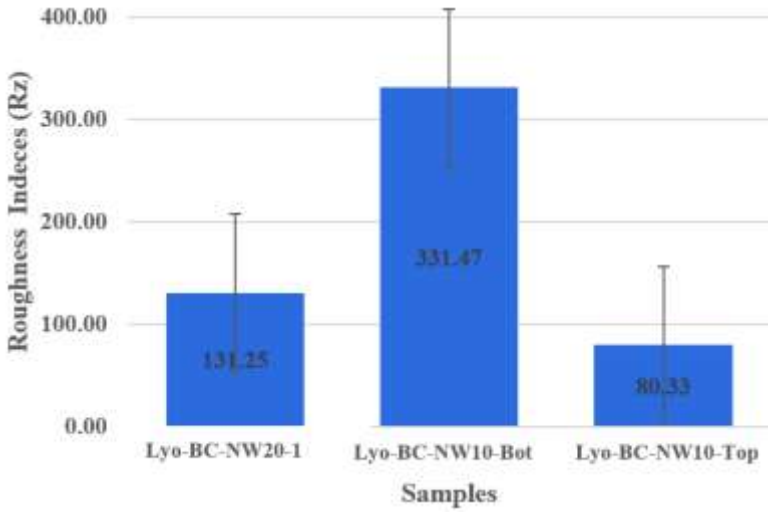

Figure 5.19 Surface roughness depth (Rz) of conventionally pre-frozen, lyophilized bacterial cellulose aerogels (samples Lyo-BC-NW20-1, Lyo-BC-NW10-Bot, and Lyo-BC-NW10-Top).

5.3.1.6 Thermal Conductivity and Thermal Resistance of Bacterial Cellulose

Thermal conductivity ranges from 0.0299 to 0.0404 $W \cdot m^{-1} \cdot K^{-1}$ (Figure 5.20), with lowest λ for Lyo-BC-NW20-1 (0.0299 $W \cdot m^{-1} \cdot K^{-1}$) and highest for Lyo-BC-NW10-Bot (0.0404 $W \cdot m^{-1} \cdot K^{-1}$); Lyo-BC-NW10-Top shows moderate λ (0.0322 $W \cdot m^{-1} \cdot K^{-1}$) and highest diffusivity (1.231 mm^2/s). Variations reflect pore structure: higher porosity and uniformity reduce heat transfer, whereas densification and fibril aggregation increase conductivity, consistent with structural analyses.

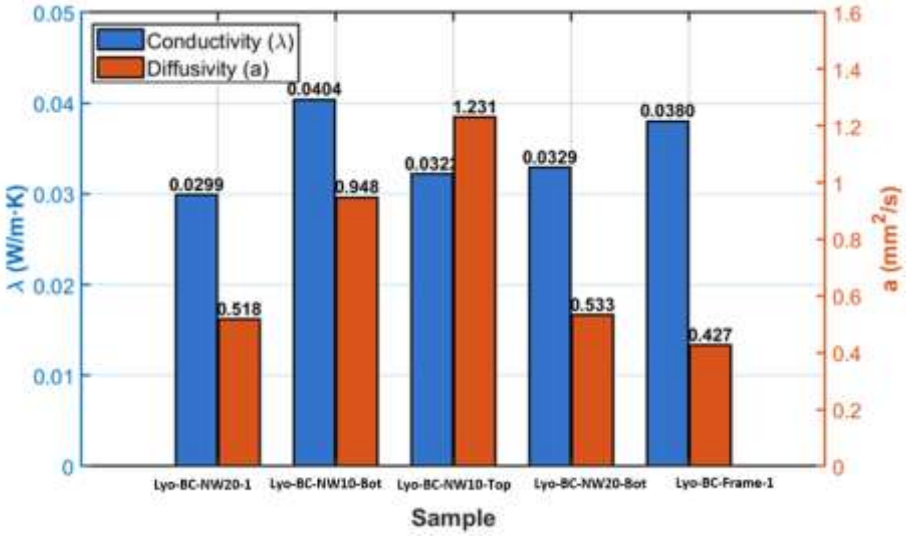

Figure 5.20 Thermal conductivity (λ) and thermal diffusivity (a) of conventionally pre-frozen, lyophilized bacterial cellulose aerogels measured by Alambeta.

5.3.1.7 Surface Wettability Evaluation of Bacterial Cellulose

Conventionally pre-frozen BC aerogels exhibit hydrophilic behavior with contact angles of 51.43°–67.92° (Figure 5.21), higher than cryogenically frozen samples (~0°), indicating reduced wettability. This is attributed to slow freezing-induced surface densification and partial pore blockage, which delays water penetration. Despite this, all samples remain hydrophilic due to the hydroxyl-rich cellulose structure, though moisture exposure may affect network stability.

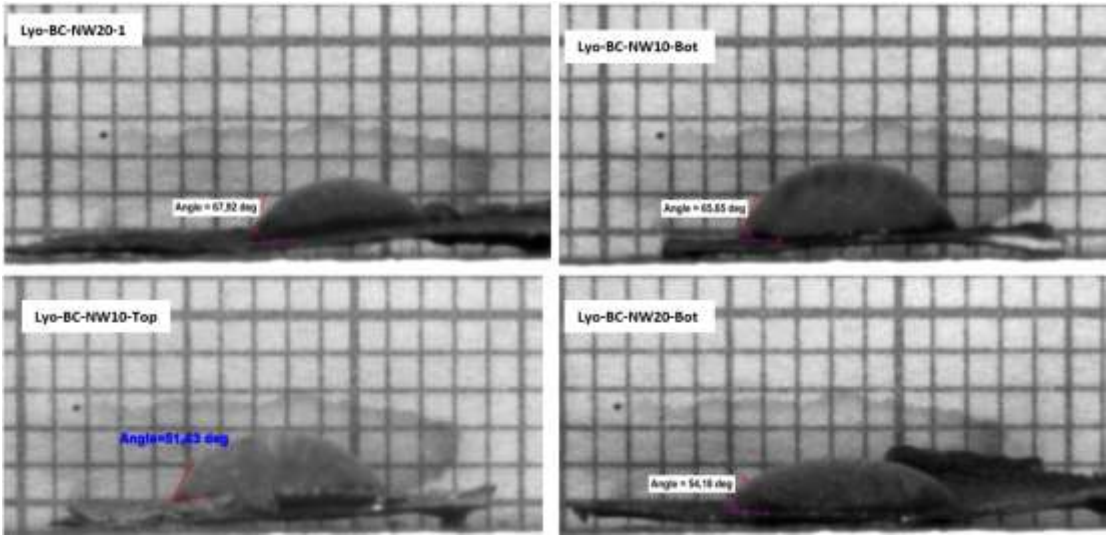

Figure 5.21 Optical microscope contact angle measurements of conventionally pre-frozen, lyophilized bacterial cellulose aerogels (BCAs) stabilized with nonwoven PES (NW) fabrics.

5.3.2 Liquid nitrogen (LN): rapid pre-freezing for freeze-drying optimization

5.3.2.1 Surface Morphology and Microstructure Analysis of Bacterial Cellulose

SEM images of LN pre-frozen samples (Lyo-BC-LN2, Figure 5.22) show a highly uniform and interconnected nanofibrillar network with homogeneous pore distribution. This structure results from rapid heat extraction during LN freezing, which promotes instant ice nucleation and suppresses crystal growth, preventing pore coarsening. The preserved fine fibrillar architecture and pore uniformity are clearly observed in both surface and cross-sectional SEM images.

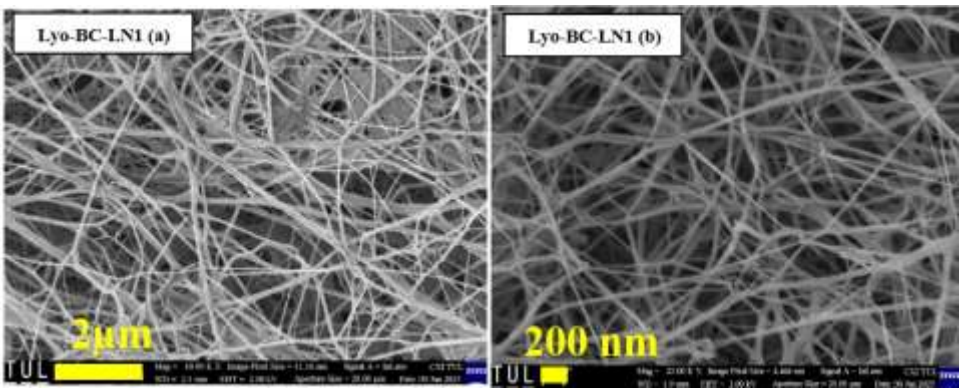

Figure 5.22 Surface (Lyo-BC-LN2-a) and Cross-sectional (Lyo-BC-LN2-b) of BCAs pre-frozen using LN.

5.3.2.2 Elemental Composition Analysis of Bacterial Cellulose

EDX results (Figure 5.23) show dominant carbon (58.3 wt%) and oxygen (41.0 wt%) with trace impurities, confirming preserved cellulose composition and chemical purity after LN freezing.

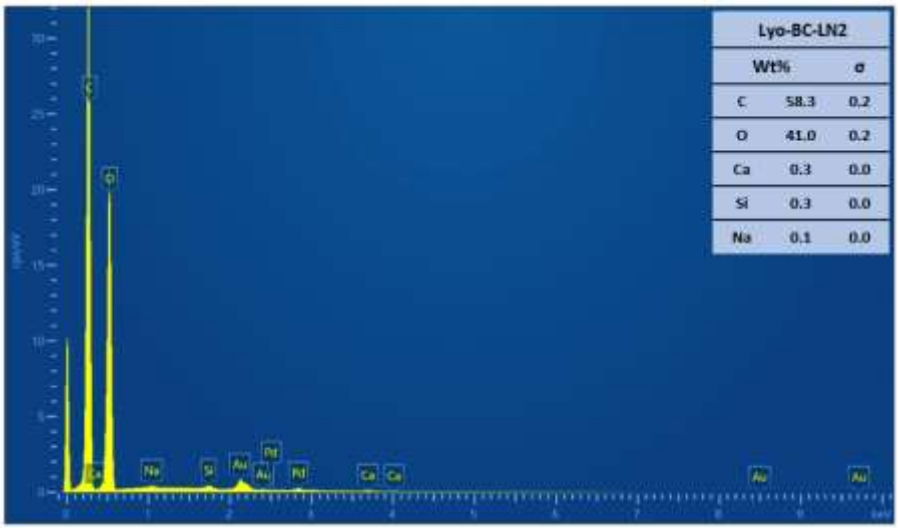

Figure 5.23 EDX spectrum of LN pre-frozen BC sample.

5.3.2.3 Geometrical Characterization of Bacterial Cellulose

LN pre-frozen samples (Table 5.5) exhibit low density (0.016–0.041 g/cm^3) and high porosity (97.34–98.97%). Lyo-BC-LN1 shows highest porosity (98.97%) and lowest density, while Lyo-BC-LN3 shows higher density due to reduced thickness. Variations arise from geometry rather than nanostructure, confirming that LN freezing preserves pore continuity and minimizes structural collapse.

Table 5.5 Geometrical analysis of LN pre-freezing used BC samples dried with lyophilization.

Samples	Description	Dry Thickness (cm)	Dry Mass (g)	Apparent Volume (cm^3)	Volume of Cellulose (cm^3)	Porosity (%)	Sample size (cm)	Shape
Lyo-BC-LN1	LN pre-freezing using BC film	0.72	2.92	182.13	1.87	98.97	13.6x18.6	Rectangular
Lyo-BC-LN2		0.49	3.68	154.35	2.36	98.47	14x22.5	Rectangular
Lyo-BC-LN3		0.27	3.85	92.91	2.47	97.34	15.5x22.2	Rectangular

5.3.2.4 Compression Test

LN pre-frozen BC aerogels (Figure 5.24) show nonlinear compressive behavior typical of porous networks. Lyo-BC-LN1 exhibits higher stiffness (~16–17 N at 30% strain), while Lyo-BC-LN2 shows greater deformation (~60% strain at ~35 N). Differences arise from geometry and porosity, where thicker, highly porous structures enhance load transfer, and thinner samples deform more before densification. The behavior is consistent with geometrical data and reflects the influence of pore architecture and fibril connectivity, which may vary slightly due to biological formation and freezing-induced structuring.

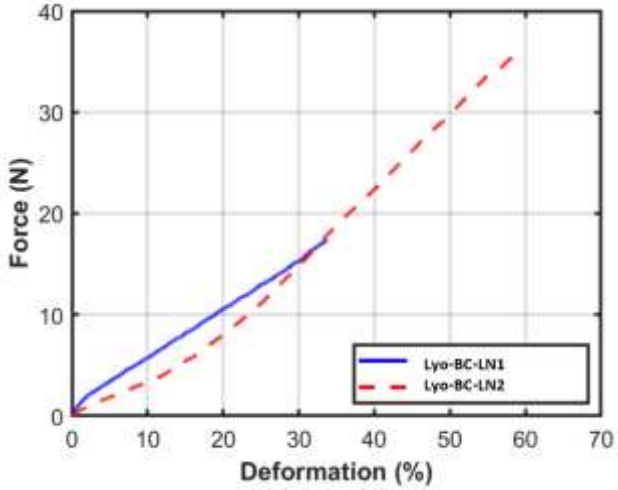

Figure 5.24 Force-deformation curve of lyophilized bacterial cellulose aerogels (samples Lyo-BC-LN1 and Lyo-BC-LN2).

5.3.2.5 3D Surface Roughness and Topography Analysis of Bacterial Cellulose

Surface roughness (Figure 5.25) shows relatively smooth surfaces for Lyo-BC-LN1 and LN3 (Rz = 39.04–45.15 µm), while Lyo-BC-LN2 exhibits higher roughness (Rz = 209.22 µm). Variations reflect freezing-induced pore formation, where LN freezing preserves nanoscale structure but may induce localized macroporosity depending on sample geometry.

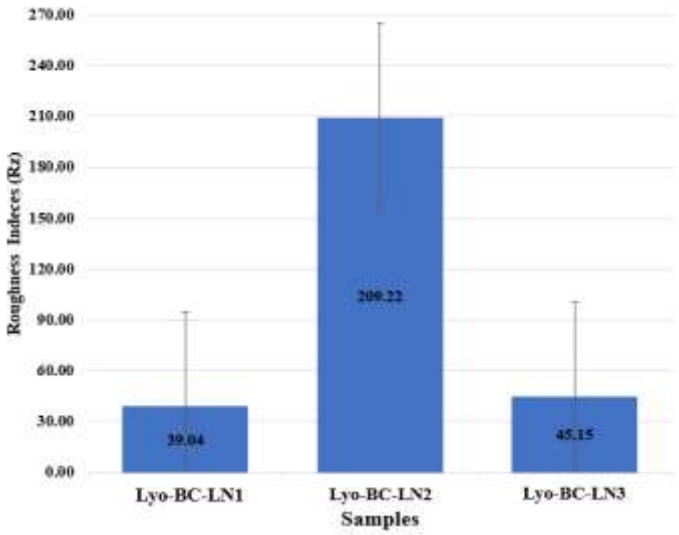

Figure 5.25 BC samples pre-frozen using LN.

5.3.2.6 Thermal Conductivity and Thermal Resistance of Bacterial Cellulose

Thermal conductivity decreases from Lyo-BC-LN1 (0.0448 $W \cdot m^{-1} \cdot K^{-1}$; a = 5.784 $mm^2 \cdot s^{-1}$) to LN2 (0.0383 $W \cdot m^{-1} \cdot K^{-1}$; 2.745 $mm^2 \cdot s^{-1}$) and LN3 (0.0349 $W \cdot m^{-1} \cdot K^{-1}$; 1.071 $mm^2 \cdot s^{-1}$) (Figure 5.26), indicating improved insulation with increasing porosity and reduced solid-phase contribution. Trends align with structural analyses, confirming effective thermal insulation of LN-assisted cryogels.

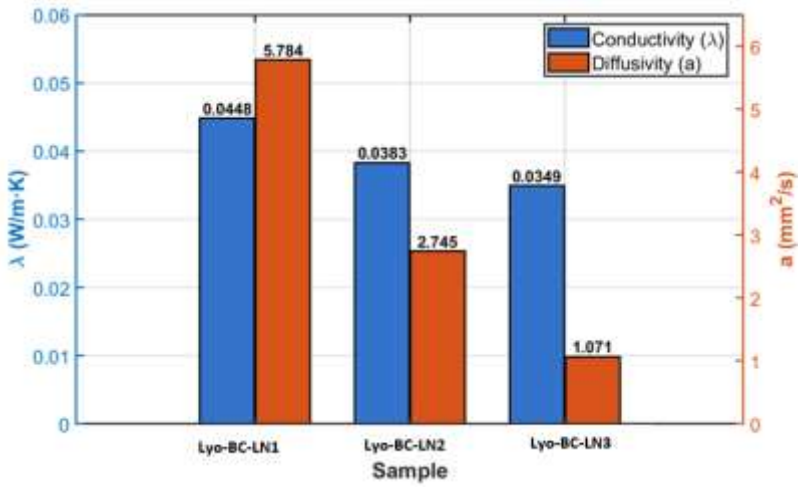

Figure 5.26 Thermal conductivity and diffusivity of BC samples pre-frozen using LN before lyophilization.

5.3.3 In-Situ Freezing in the Lyophilizer

5.3.3.1 Surface Morphology and Microstructure Analysis of Bacterial Cellulose

SEM analysis (Figure 5.27) shows that in-situ frozen BC cryogels (Lyo-BC-NS-1, NS-2, NS-3) exhibit a highly porous, interconnected nanofibrillar network with sponge-like macropores and continuous pore channels across multiple scales.

This structure results from controlled shelf freezing, which stabilizes the hydrogel during ice formation and prevents collapse, preserving both microscale porosity and nanoscale fibrillar organization.

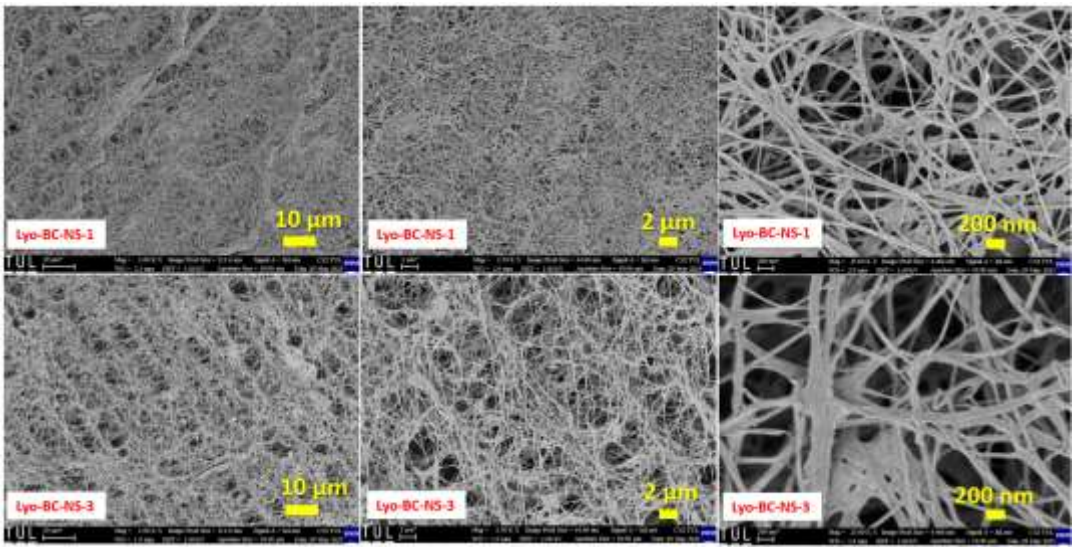

Figure 5.27 SEM images comparing BC cryogels at different magnifications.

Quantitative analysis (Figure 5.28) shows fibril diameters of ~26–77 nm (NS-1) and ~34–84 nm (NS-3), with inter-fibrillar spacing up to ~700 nm, confirming preserved nanoscale architecture. Minor differences between samples are attributed to local variations in fibril packing, rather than structural changes.

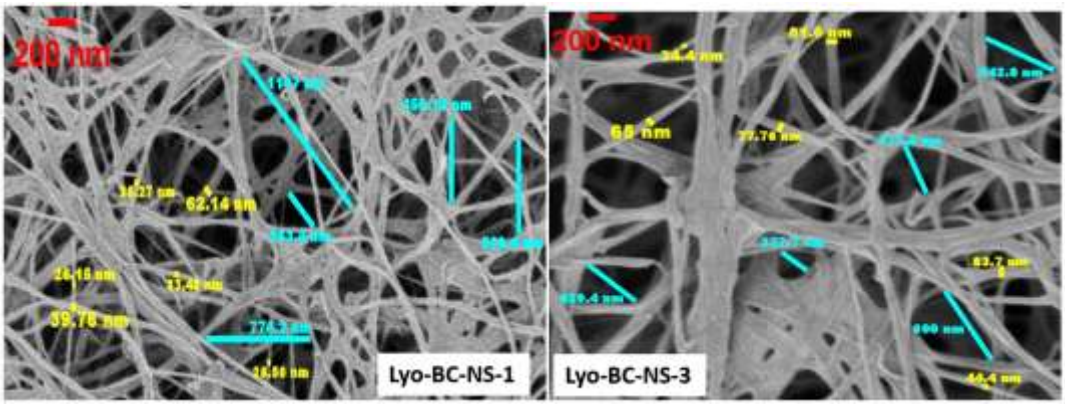

Figure 5.28 Diameter of fibers in BC cryogels.

5.3.3.2 Elemental Composition Analysis of Bacterial Cellulose

EDX analysis of Lyo-BC-NS-3 (Figure 5.29) shows dominant carbon (51.4 wt%) and oxygen (47.5 wt%), confirming the cellulose structure, with minor traces of Ca (0.5%), Na (0.3%), Si (0.2%), and S (0.1%).

These trace elements are attributed to residual minerals from the tea-based medium rather than processing contamination, consistent with literature reports on biogenic BC [50]. The compositional results align with SEM observations, where the cryogel maintains a porous network with some localized densification and fibril bundling.

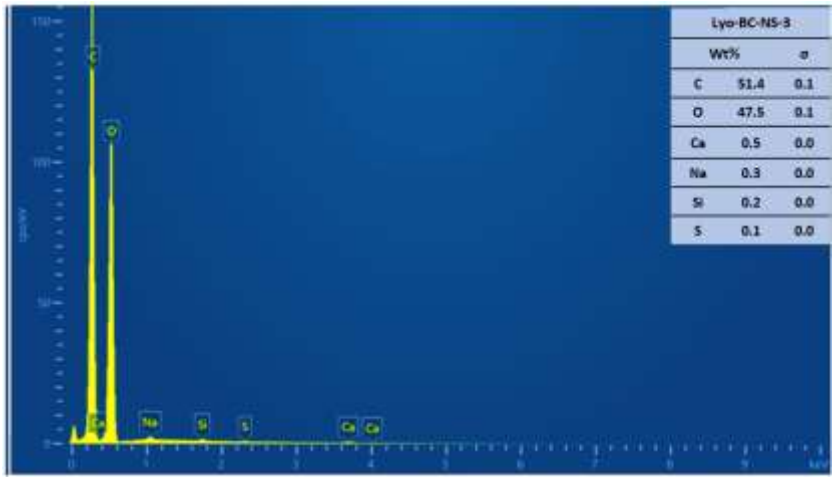

Figure 5.29 EDX spectrum of sample Lyo-BC-NS-3 of bacterial cellulose cryogel.

5.3.3.3 Geometrical Analysis

Lyophilized BC cryogels (Lyo-BC-NS-1 to NS-3) show ultra-low density (0.012–0.029 g/cm³) and high porosity (98.14–99.22%) (Table 5.6), indicating effective preservation of the 3D network after sublimation of >99% water. Variations arise from initial thickness and mass but do not affect overall structural integrity. Results are consistent with reported ranges (ρ ≈ 0.013–0.028 g/cm³; porosity ≈ 98.18–99.2%) [39], confirming that lyophilization reliably produces highly porous cryogels, while freezing and support conditions influence uniformity.

Table 5.6 Geometrical analysis of BC samples dried with lyophilization.

Sample No	Drying Method	Before Drying			After Drying					
		Wet Thickness (cm)	Wet Mass (g)	Sample size (cm)	Dry Thickness (cm)	Dry Mass (g)	Apparent Volume (cm^3)	Volume of Cellulose (cm^3)	Porosity (%)	Sample size (cm)
Lyo-BC-NS-1	Lyophilization	0.28	31.44	10x10	0.13	0.34	11.7	0.22	98.14	9x10
Lyo-BC-NS-2		0.65	78.38	10x10	0.57	0.73	53.63	0.47	99.13	9.6x9.8
Lyo-BC-NS-3		0.81	181.5	13.5 x 14.2	0.67	1.42	116.68	0.91	99.22	12.9x13.5

5.3.3.4 Functional Group and Chemical Structure Analysis of Bacterial Cellulose

FTIR spectra (Figure 5.30) confirm preservation of cellulose I structure (O–H ~3340 cm^{-1}, C–H ~2890 cm^{-1}, C–O 1160–1030 cm^{-1}) with no degradation.

Differences arise in hydrogen bonding and hydration state:

- **Lyo-BC-NS-1** → broader O–H band → higher bound water / less crystalline domains
- **Lyo-BC-NS-3** → closer to $ScCO_2$ aerogels → more stable hydrogen-bond network

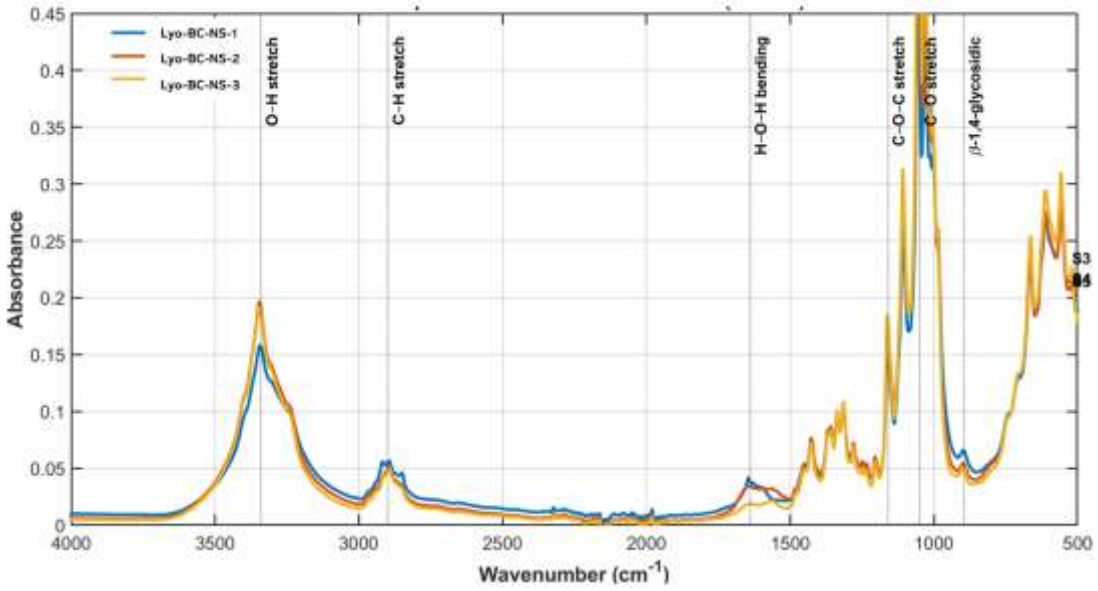

Figure 5.30 FT-IR analysis of bacterial cellulose cryogels.

5.3.3.5 3D Surface Roughness and Topography Analysis of Bacterial Cellulose

CLSM analysis (Figure 5.31) shows cryogels (Lyo-BC-NS-1, Lyo-BC-NS-3) exhibit intermediate roughness (Rz = 30.05 and 27.80 µm), reflecting heterogeneous surfaces formed by freezing-induced stress and sublimation-driven restructuring. Lyo-BC-NS-1 shows greater waviness (−49 to +47 µm, Figure 5.32) linked to partial collapse, while Lyo-BC-NS-3 presents a denser, flattened surface due to pore wall amalgamation.

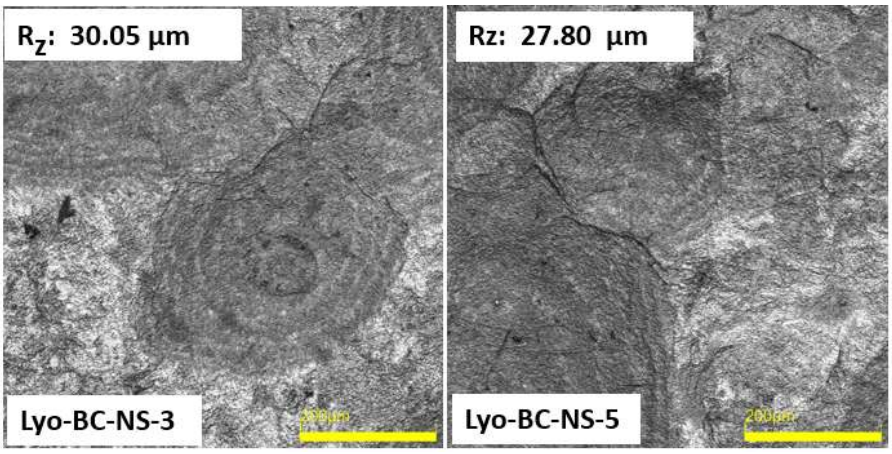

Figure 5.31 Analysis of surface roughness of cryogels. Objective: 20× for all images. The scale bar indicates 200 µm. Rz: average roughness depth.

Comparative analysis (Figures 5.9, 5.32) indicates $ScCO_2$ aerogels maintain smoother, more isotropic networks, whereas freeze-drying introduces localized densification and surface irregularity [38]. Statistical evaluation (Figure 5.33, Tables 5.7–5.8; ANOVA F = 5.28, p = 0.0267) confirms significant differences, with highest roughness in Sc-BC-NS-1 (58.04 µm), lowest in Sc-BC-NS-2 (21.49 µm), and cryogels remaining intermediate (27.80–30.05 µm). Tukey analysis shows Sc-BC-NS-1 differs significantly ($p < 0.05$), while cryogels and Sc-BC-NS-2 are statistically similar.

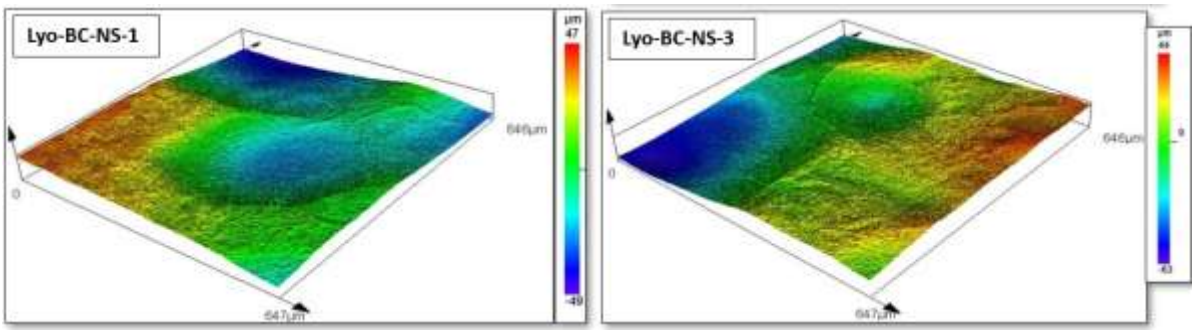

Figure 5.32 Three-dimensional surface topography of BC samples.

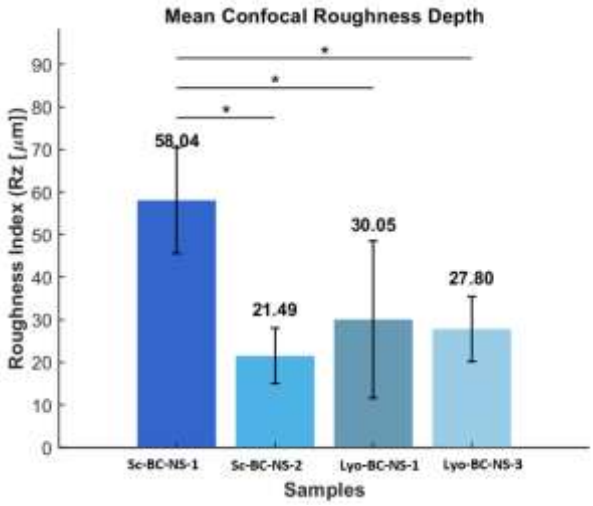

Figure 5.33 Mean confocal surface roughness (Rz [µm]) of BC aerogel and cryogel specimens (n = 3). The bars indicate the mean ± standard deviation (SD). Asterisks indicate statistically significant differences among samples ($p < 0.05$, one-way ANOVA with Tukey's post hoc test).

Table 5.7 Results of one-way ANOVA on BC samples.

ANOVA Results					
Source	SS	df	MS	F	Prob>F
Groups	2363.8	3	787.9	5.282	0.0267
Error	1193.4	8	149.2		
Total	3557.2	11			

Table 5.8 Tukey post-hoc analysis results for BC samples.

Tukey post-hoc results					
Group1	Group2	Lower	MeanDiff	Upper	pValue
{'Sc-BC-NS-1'}	{'Sc-BC-NS-2'}	4.61	36.55	68.48	0.03
{'Sc-BC-NS-1'}	{'Lyo-BC-NS-1'}	-3.94	27.99	59.93	0.09
{'Sc-BC-NS-1'}	{'Lyo-BC-NS-3'}	-1.70	30.24	62.17	0.06
{'Sc-BC-NS-2'}	{'Lyo-BC-NS-1'}	-40.49	-8.55	23.38	0.83
{'Sc-BC-NS-2'}	{'Lyo-BC-NS-3'}	-38.25	-6.31	25.63	0.92
{'Lyo-BC-NS-1'}	{'Lyo-BC-NS-3'}	-29.69	2.24	34.18	1.00

Overall, surface morphology is governed by both drying pathway and pre-processing conditions, with cryogels exhibiting intermediate roughness and partial structural compaction between uniform aerogels and heterogeneous freeze-derived structures.

5.3.3.6 Surface Area and Porosity Characterization of Bacterial Cellulose

BET analysis (Table 5.9) shows cryogels with moderate surface area (40.09–62.99 m^2/g; mean 51.43 m^2/g) and low pore volume (0.08–0.17 cm^3/g; mean 0.13 cm^3/g), with mesopore diameters ~10.6 nm, indicating reduced porosity and structural variability. This results from limited freezing control, leading to non-uniform ice templating, fibril aggregation, pore coalescence, and partial network collapse.

Table 5.9 BET measurements of BC cryogels.

Sample	Drying Method	BET Surface Area (m^2/g)	Total Pore Volume (cm^3/g)	Average Pore Diameter (nm)
Lyo-BC-NS-1	Freeze-dried	40.09	0.08	9.8
Lyo-BC-NS-2		62.99	0.17	9.8
Lyo-BC-NS-3		51.2	0.13	12.2
Mean		51.43	0.13	10.6
Standard Deviation		11.45	0.045	1.38

Isotherms (Figure 5.34) exhibit Type IV with H3 hysteresis, confirming slit-like mesopores and capillary condensation at $p/p_o \approx 0.8–0.9$. Lyo-BC-NS-1 shows lowest uptake (SBET ≈ 40 m^2/g) indicating pore blockage, Lyo-BC-NS-2 shows higher uptake (≈63 m^2/g) with improved but less uniform mesoporosity, and Lyo-BC-NS-3 shows larger pores (~12 nm) due to pore coalescence.

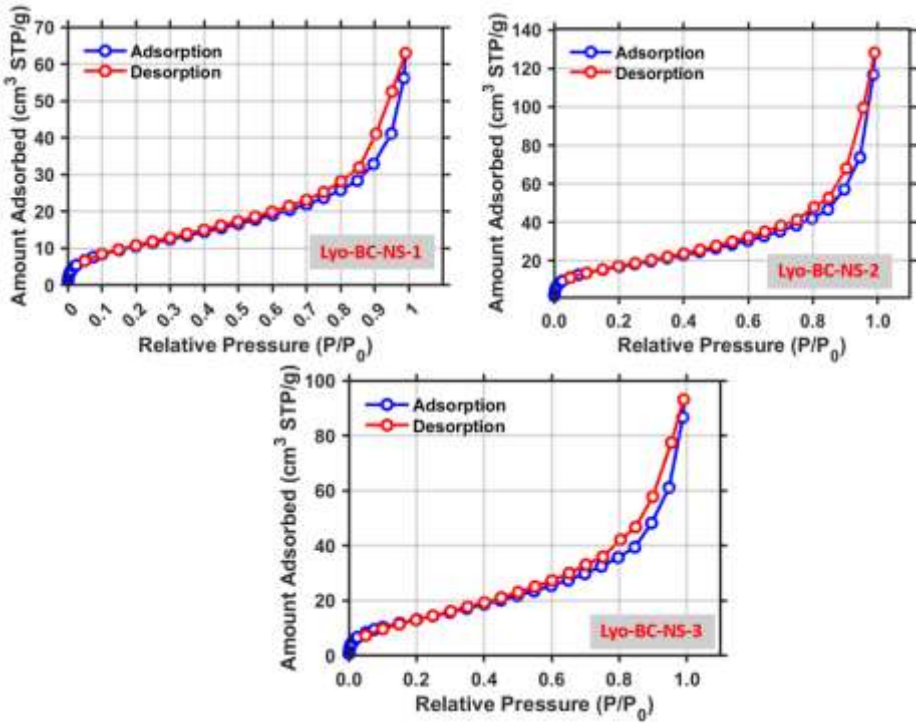

Figure 5.34 N_2 adsorption-desorption isotherms of the BC specimens.

Overall, cryogels exhibit lower surface area and pore volume than aerogels, consistent with partial structural compaction observed in morphological analyses.

5.3.3.7 Thermal Transition and Heat Flow Analysis of Bacterial Cellulose Samples

DSC analysis (Figure 5.35) shows high thermal variability among cryogels, linked to structural heterogeneity (thickness 0.13–0.67 cm; SBET ~40–63 m^2/g; Vp 0.08–0.17 cm^3/g). Non-uniform freezing produces irregular pore structures and partial collapse, resulting in structure-dependent heat flow. Lyo-BC-NS-1 exhibits broader transitions indicating lower porosity and higher disruption, while NS-2 and NS-3 show more stable profiles with partial structural preservation. In contrast, $ScCO_2$-dried samples exhibit uniform DSC behavior due to homogeneous pore networks.

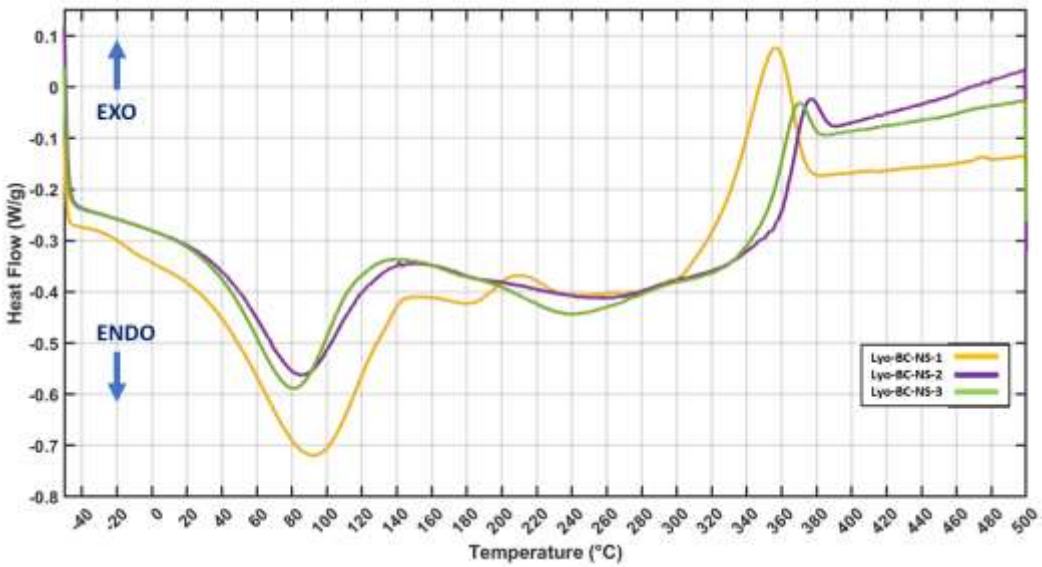

Figure 5.35 DSC results of cryogel samples.

5.3.3.8 Thermal Conductivity and Thermal Resistance of Bacterial Cellulose

Thermal conductivity varies from 0.030 W/m·K (NS-1) to 0.041 W/m·K (NS-3), with diffusivity increasing from 1.72 to 8.28 mm²/s (Figure 5.36). Lower values in NS-1 indicate reduced heat transfer due to less connected pore structures, while higher values in NS-2 and NS-3 reflect increased structural continuity from thickness-dependent freezing effects. Compared to $ScCO_2$ aerogels (λ ≈ 0.040–0.042 W/m·K; higher diffusivity), cryogels—especially thinner samples—provide improved thermal insulation due to reduced heat propagation pathways.

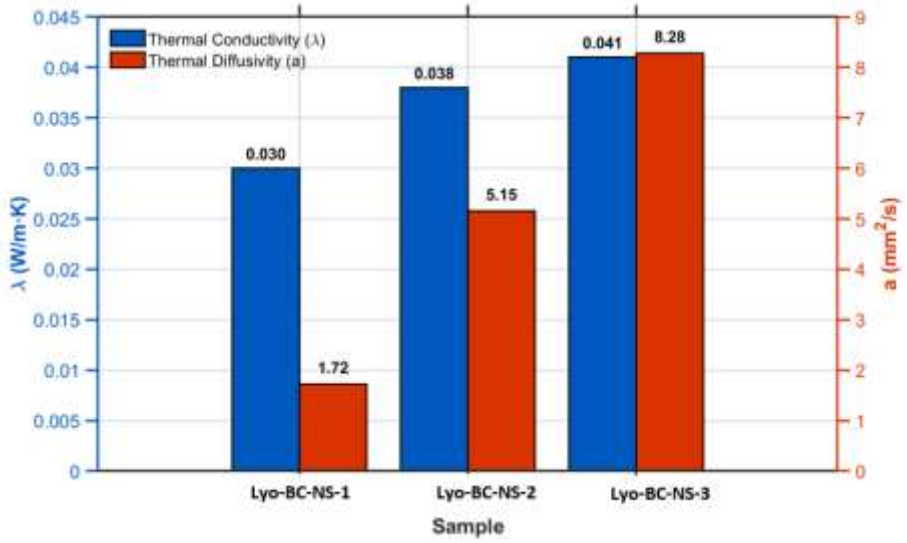

Figure 5.36 Thermal conductivity and diffusivity of cryogel samples.

5.3.3.9 Monitoring of Environmental Conditioning Parameters (Temperature and Relative Humidity)

Environmental monitoring (Figure 5.37) confirms stable conditions during testing, with temperature ~26.8–27.7 °C (σ = 0.18–0.40) and humidity ~32–35% RH across all samples. This stability indicates that observed material differences are not driven by external conditions, but rather by processing-induced structural variation and intrinsic biological variability, which can influence fibril arrangement and pore formation during drying.

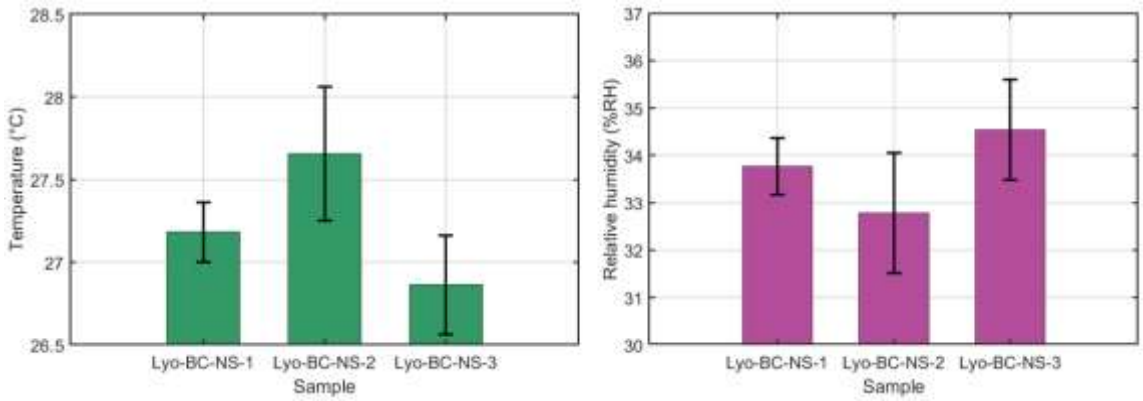

Figure 5.37 Thermal and humidity distribution of cryogel samples (left: temperature fluctuation; right: humidity fluctuation image).

5.3.3.10 Frequency-Dependent Sound Absorption Coefficient of Bacterial Cellulose

Sound absorption spectra (Figure 5.38) show low-to-moderate performance across 100–5000 Hz with clear frequency dependence. At low frequencies (100–1000 Hz), absorption remains weak (SAC ≈ 0.023–0.042 at 1000 Hz; Table 5.10) due to limited thickness relative to wavelength, with only slight improvement as thickness increases (~0.13–0.67 cm).

At higher frequencies (~4000 Hz), absorption increases (SAC ≈ 0.079–0.147), indicating enhanced interaction between sound waves and the porous structure. Measurements above ~5000 Hz show instability due to impedance tube limitations and are excluded from analysis.

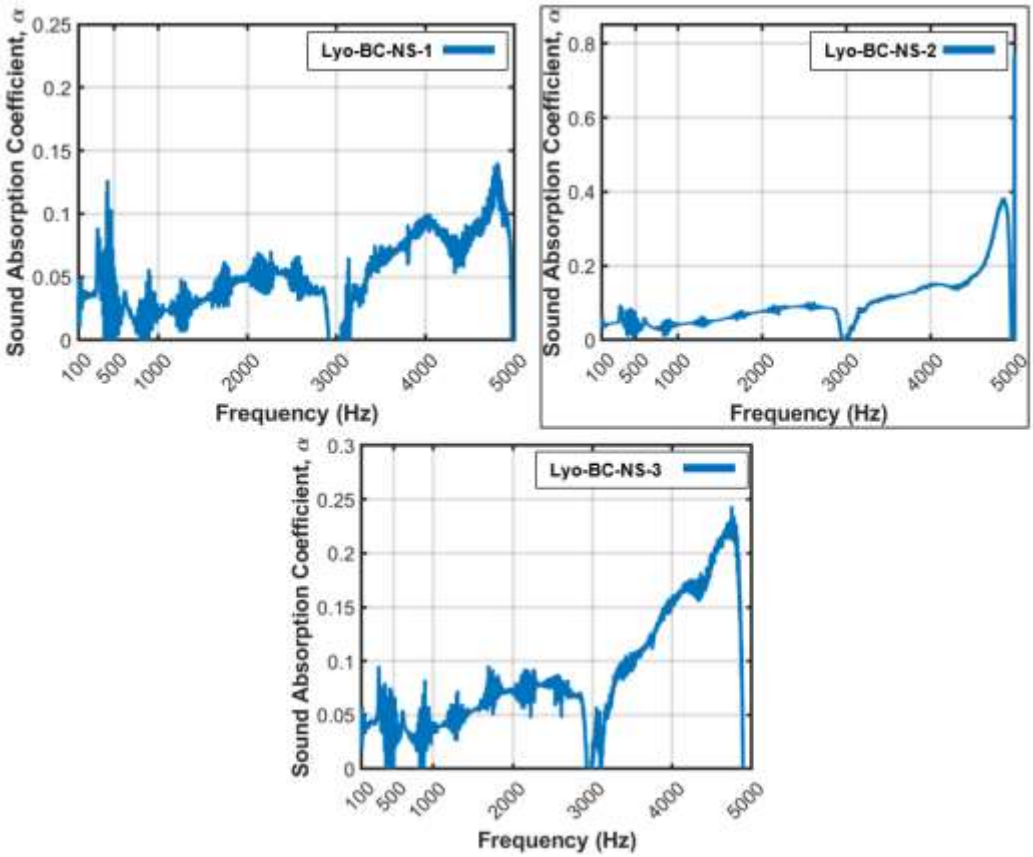

Figure 5.38 Frequency range spectrum of sound absorption coefficient of cryogel samples.

Table 5.10 Band-averaged SAC values for cryogel samples.

Sample	Center Frequency (Hz)	Band (Hz)	SAC	Thickness (cm)
Lyo-BC-NS-1	1000	891-1122	0.023	0.13
	4000	3548-4466	0.079	
	5000	4466-5623	0.000	
Lyo-BC-NS-2	1000	891-1122	0.042	0.57
	4000	3548-4466	0.140	
	5000	4466-5623	0.000	
Lyo-BC-NS-3	1000	891-1122	0.038	0.67
	4000	3548-4466	0.147	
	5000	4466-5623	0.000	

Overall, cryogels exhibit gradual frequency-dependent absorption with moderate thickness influence and stable behavior within the valid measurement range.

5.3.4 Regenerated BC Pellicles obtained via mechanical disintegration

5.3.4.1 Surface Morphology and Microstructure Analysis of Bacterial Cellulose

SEM analysis (Figure 5.39) shows Lyo-RBC with a porous but heterogeneous network composed of thicker fibril bundles and localized densification, contrasting with the uniform native BC structure. Mechanical disintegration disrupts the

hierarchical network, and limited freezing promotes fibril aggregation, coalescence, and partial collapse, resulting in reduced nanoscale uniformity and accessible surface area while maintaining connectivity.

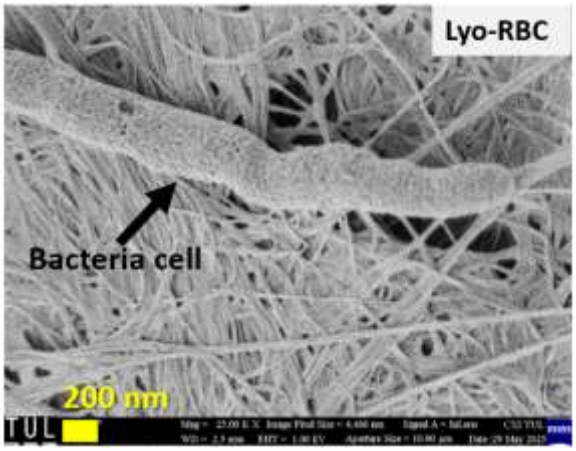

Figure 5.39 SEM image of regenerated BC aerogel.

5.3.4.2 Elemental Composition Analysis of Bacterial Cellulose

EDX analysis (Figure 5.40) confirms cellulose composition (C: 52.5 wt%, O: 46.4 wt%) with minor trace elements from biogenic sources, indicating preserved chemical integrity after regeneration.

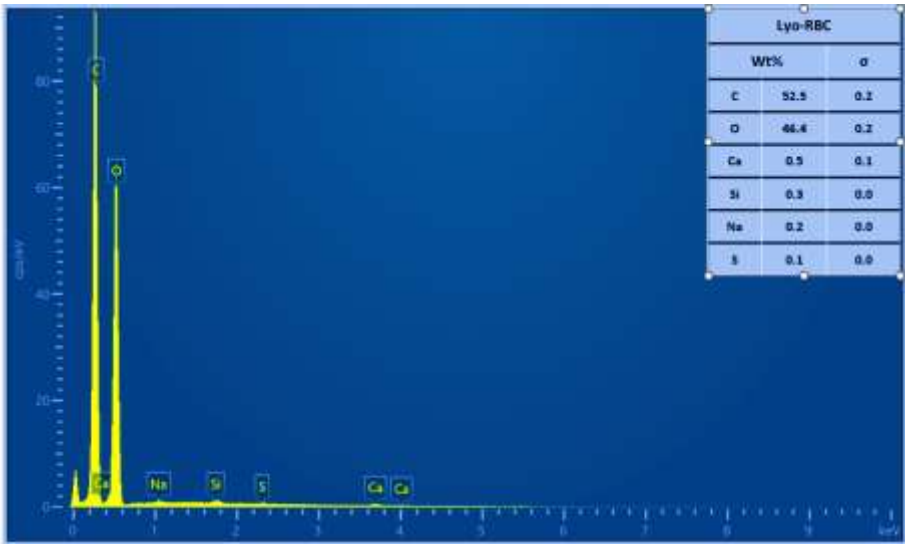

Figure 5.40 EDX spectrum of the Lyo-RBC sample.

5.3.4.3 3D Surface Roughness and Topography Analysis of Bacterial Cellulose

Confocal analysis (Figure 5.41) shows very high surface roughness (Rz ≈ 197 µm) with pronounced heterogeneity, caused by mechanical disintegration, fibril reassembly, and uncontrolled ice templating. This results in non-uniform shrinkage,

surface collapse, and macro-scale wrinkling, consistent with SEM observations of reduced structural uniformity.

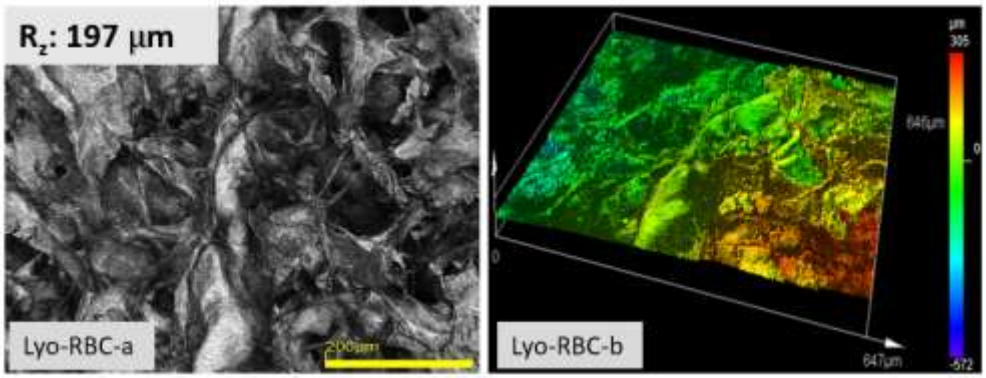

Figure 5.41 Confocal scanning microscope images of the Lyo-RBC sample (a) Roughness Depth (b) 3D topography map.

5.3.4.4 Surface Area and Porosity Characterization of Bacterial Cellulose

BET analysis (Table 5.11) shows low surface area (31.1 m^2/g), pore volume (0.16 cm^3/g), and large mesopore diameter (23.36 nm), indicating reduced nanoscale porosity due to fibril aggregation and pore coalescence. The isotherm (Figure 5.42) exhibits Type IV behavior with hysteresis (P/P_o > 0.8), confirming mesoporosity dominated by enlarged voids. These results align with SEM and roughness data, indicating structural densification and heterogeneous pore architecture.

Table 5.11 BET result of the regenerated BC sample.

Sample	Drying Method	BET Surface Area (m^2/g)	Total Pore Volume (cm^3/g)	Average Pore Diameter (nm)
Lyo-RBC	Freeze-drying	31.1	0.16	23.36

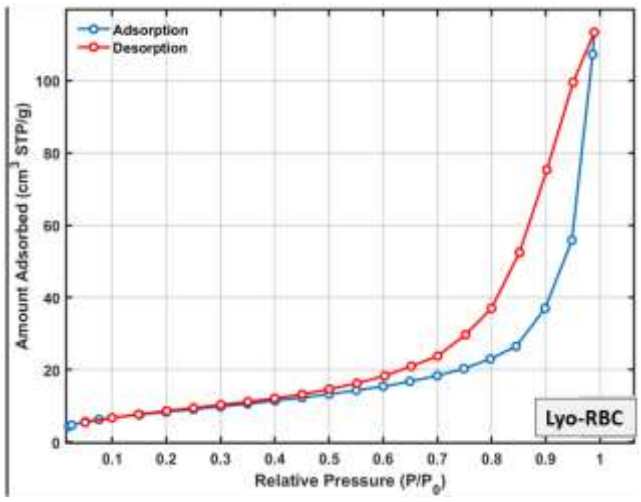

Figure 5.42 BET adsorption-desorption analysis of Lyo-RBC sample.

5.3.4.5 Thermal Conductivity and Thermal Resistance of Bacterial Cellulose

Thermal analysis (Figure 5.43) shows low conductivity (λ = 0.04 $W \cdot m^{-1} \cdot K^{-1}$) and moderate diffusivity (α = 3.214 mm^2/s), reflecting reduced heat transfer due to porous structure and air-filled voids, while remaining fibrillar connectivity enables heat propagation. Results are consistent with BET (31.1 m^2/g; 0.16 cm^3/g; 23.36 nm) and SEM, indicating mesoporosity-driven phonon scattering and coarsened fiber networks.

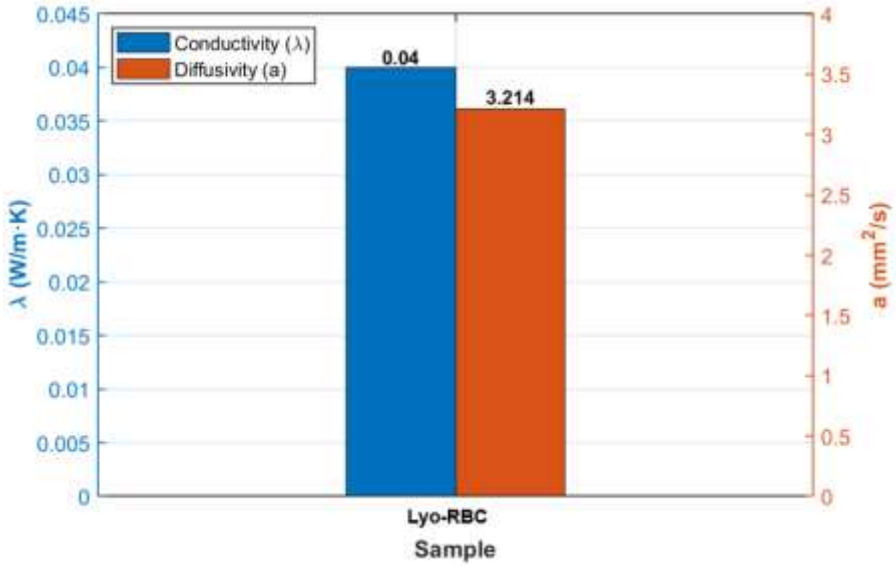

Figure 5.43 Thermal conductivity and diffusivity of the regenerated BC sample.

5.3.4.6 Functional Group and Chemical Structure Analysis of Bacterial Cellulose

FTIR (Figure 5.44) confirms preservation of cellulose structure (O–H, C–H, bound water, C–O, β-linkages), indicating that regeneration alters microstructure but not chemical composition. Property changes are therefore governed by fibril merging and pore restructuring rather than chemical modification.

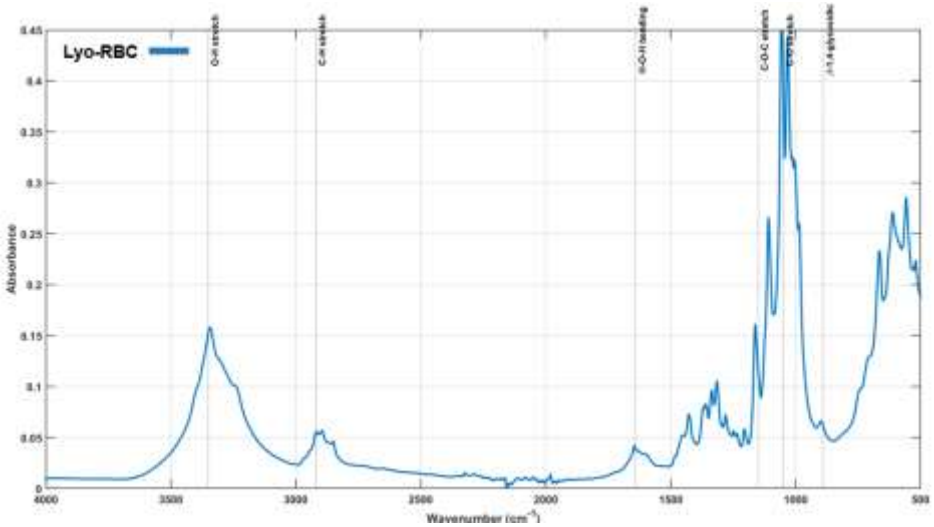

Figure 5.44 FT-IR analysis of Lyo-RBC.

5.3.4.7 Frequency-Dependent Sound Absorption Coefficient of Bacterial Cellulose

Acoustic response (Figure 5.45; Table 5.12) shows frequency-dependent behavior, with low absorption at 1000 Hz (SAC ≈ 0.085), peak at 4000 Hz (≈0.68), and decline at 5000 Hz (≈0.34). Low-frequency performance is limited by thickness, while mid-frequency enhancement arises from viscous–thermal dissipation within mesopores [51,52]. The peak (3.5–4.5 kHz) reflects effective pore–wave interaction, while high-frequency reduction is linked to boundary and measurement effects [53(p. 1998)].

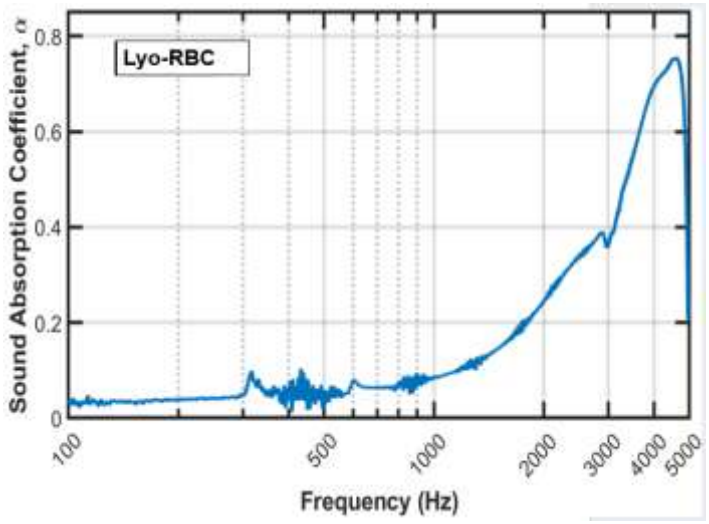

Figure 5.45 Frequency range spectrum of sound absorption coefficient of the Lyo-RBC Sample.

Table 5.12 Band-averaged SAC values for regenerated BC Aerogel sample.

Sample	Center Frequency (Hz)	Band (Hz)	SAC
Lyo-RBC	1000	891-1122	0.085
	4000	3548-4466	0.68
	5000	4466-5623	0.34

Overall, regenerated Lyo-RBC combines reduced surface area, enlarged mesoporosity, and preserved chemistry, resulting in low thermal conductivity, moderate diffusivity, and enhanced mid-frequency acoustic absorption governed by fibril aggregation and pore restructuring.

5.4 Structural Feasibility of Crystalline Graphite Incorporation with BC

Macroscopic observation (Figure 5.46) shows a color transition from translucent brown to opaque black, confirming homogeneous graphite dispersion within the BC matrix and successful composite formation.

Figure 5.46 Macroscopic appearance of Lyo- Ref-RBC and Lyo-Graphite-RBC (a-after drying, b-before drying).

5.4.1 Morphological and Elemental Characterization of Regenerated BC Incorporation with Crystalline Graphite

SEM (Figure 5.47) shows that Lyo-Ref-RBC has a compact fibrillar network, while Lyo-Graphite-RBC exhibits increased heterogeneity and localized densification due to graphite occupying inter-fibrillar spaces and altering pore architecture.

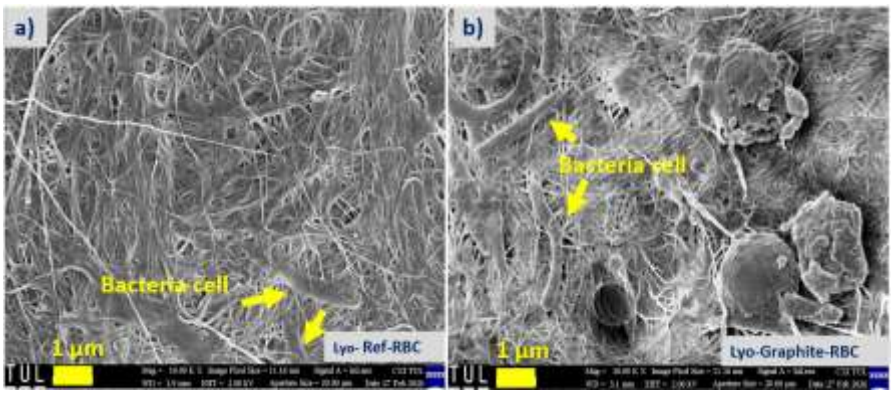

Figure 5.47 SEM images of regenerated bacterial cellulose a) RBC1-reference b) RBC2-incorporated crystalline graphite.

EDX (Figure 5.48) confirms increased carbon content (74.4 → 82.8 wt%) and reduced oxygen (24.8 → 14.7 wt%), verifying graphite incorporation; minor elements arise from residual impurities.

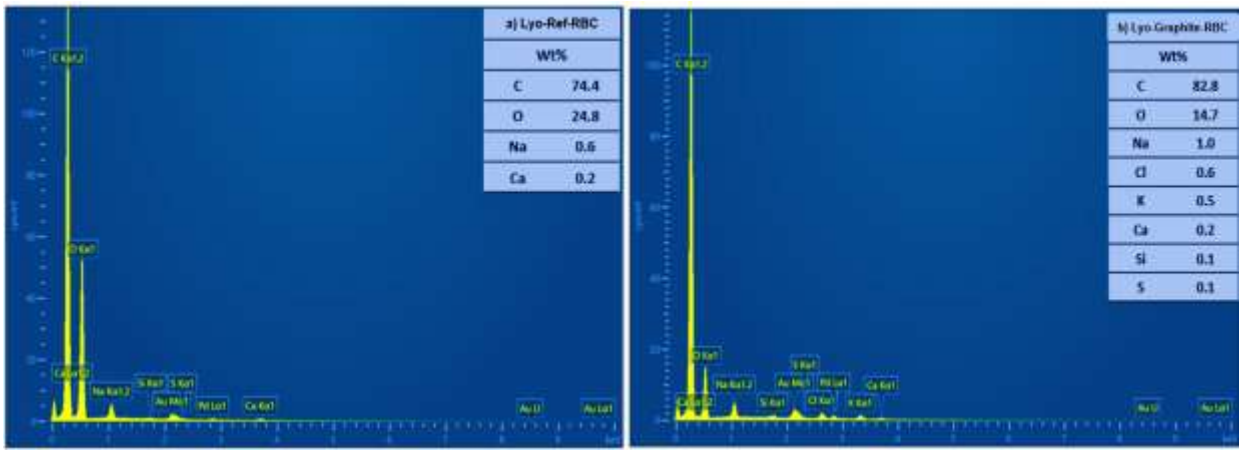

Figure 5.48 Elemental composition image of Lyo- Ref-RBC (a) and Lyo-Graphite-RBC (b).

5.4.2 Functional Group and Chemical Structure Analysis of Regenerated BC Incorporation with Crystalline Graphite

FTIR spectra (Figure 5.49) show preserved cellulose bands in both samples, confirming unchanged chemical structure. The graphite-containing sample exhibits baseline distortion due to IR attenuation/scattering, without new functional groups, indicating physical incorporation governed by interfacial contact rather than chemical bonding.

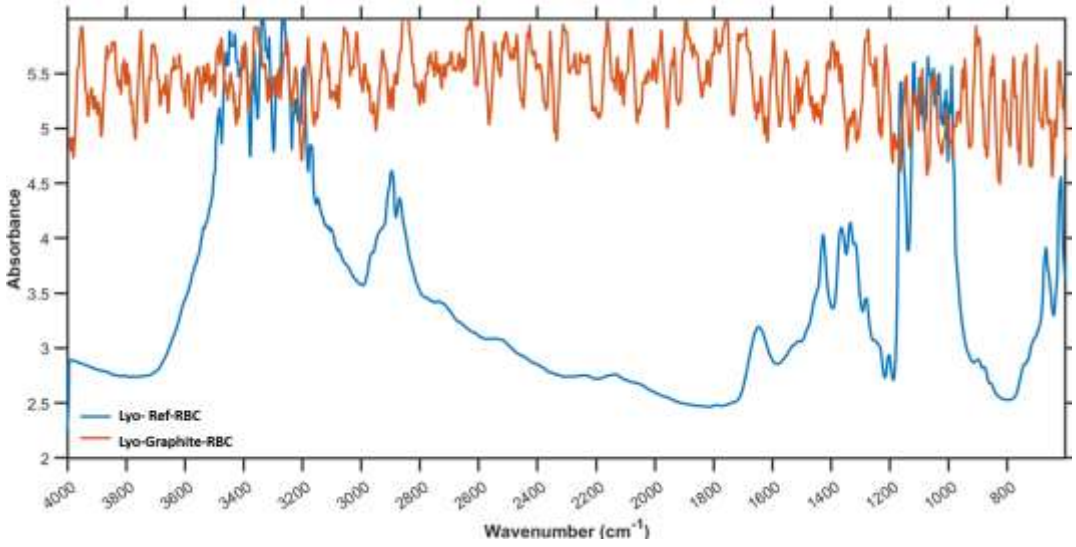

Figure 5.49 FT-IR result of Lyo- Ref-RBC and Lyo-Graphite-RBC.

Overall, graphite incorporation is structurally feasible, producing a heterogeneous BC composite with increased carbon content and modified pore architecture while preserving cellulose chemistry.

6. Conclusion

The results of this thesis demonstrate that the structural and functional performance of additive-free bacterial cellulose (BC) is primarily governed by the drying pathway and processing conditions, while chemical composition remains unchanged. Variations in microstructure, porosity, thermal, and acoustic behavior arise from drying-induced stresses, freezing kinetics, and solvent-exchange processes controlling pore preservation and nanofibrillar organization. Intrinsic biological variability in BC biosynthesis introduces minor but unavoidable differences in fibril formation, influencing material response even under standardized conditions. Room-temperature drying leads to capillary-driven densification ($\rho \approx 0.63$ g/cm^3; porosity ≈ 59.4%), whereas supercritical CO_2 drying preserves the native network, producing ultralow-density aerogels (~0.01 g/cm^3) with >99% porosity and highest surface area (~123–124 m^2/g; Vp ~0.35–0.36 cm^3/g), though with slightly higher thermal conductivity (~0.040–0.042 W·m^{-1}·K^{-1}). Freeze-drying generates ice-templated structures, where pre-freezing controls pore architecture, yielding cryogels with the lowest thermal conductivity (~0.030 W·m^{-1}·K^{-1}). In contrast, regenerated BC exhibits enhanced acoustic performance (SAC ≈ 0.68), associated with fibril bundling, increased roughness, and reduced surface area (~31 m^2/g). Preliminary graphite incorporation confirms composite feasibility without altering cellulose chemistry. Overall, distinct structure–property trade-offs are established: ambient drying induces densification, $ScCO_2$ maximizes porosity, freeze-drying optimizes insulation, and regeneration enhances acoustic absorption, identifying drying strategy and structural preservation as the key parameters for application-oriented BC design.

7. Proposed Future Activities

Surface modification & stability: Hydrophobization, plasma treatment, carbonization, and humidity-resistance studies.
Scale-up: Larger panels and continuous freeze-drying for process validation.
Applications: Oil absorption, filtration, insulation systems, and carbon-based composites for multifunctional performance.

8. References

1. Sozcu, S., Venkataraman, M., Tomková, B., & Militký, J. (2025). Biodegradability and Environmental Impact of Bacterial Cellulose. In J. Militký & M. Venkataraman (Eds.), *Fibrous Structures for Sustainable Future* (pp. 205–222). Springer Nature. https://doi.org/10.1007/978-981-95-1382-6_9
2. Leal Filho, W., Perry, P., Heim, H., Dinis, M. A. P., Moda, H., Ebhuoma, E., & Paço, A. (2022). An overview of the contribution of the textiles sector to climate change. *Frontiers in Environmental Science*, *10*. https://doi.org/10.3389/fenvs.2022.973102
3. *The impact of textile production and waste on the environment (infographics)*. (2020, December 29). Topics | European Parliament. https://www.europarl.europa.eu/topics/en/article/20201208STO93327/the-impact-of-textile-production-and-waste-on-the-environment-infographics

4. Ummartyotin, S., & Manuspiya, H. (2015). A critical review on cellulose: From fundamental to an approach on sensor technology. *Renewable and Sustainable Energy Reviews*, *41*(C), 402–412. https://doi.org/DOI:%2010.1016/j.rser.2014.08.050
5. Hamedi, H., Moradi, S., Hudson, S. M., & Tonelli, A. E. (2018). Chitosan based hydrogels and their applications for drug delivery in wound dressings: A review. *Carbohydrate Polymers*, *199*, 445–460. https://doi.org/10.1016/j.carbpol.2018.06.114
6. Farah, S., Anderson, D. G., & Langer, R. (2016). Physical and mechanical properties of PLA, and their functions in widespread applications—A comprehensive review. *Advanced Drug Delivery Reviews*, *107*, 367–392. https://doi.org/10.1016/j.addr.2016.06.012
7. Chunshom, N., Chuysinuan, P., Thanyacharoen, T., Techasakul, S., & Ummartyotin, S. (2019). Development of gallic acid/cyclodextrin inclusion complex in freeze-dried bacterial cellulose and poly (vinyl alcohol) hydrogel: Controlled-release characteristic and antioxidant properties. *Materials Chemistry and Physics*, *232*, 294–300. https://doi.org/10.1016/j.matchemphys.2019.04.070
8. Sozcu, S., Frajova, J., Wiener, J., Venkataraman, M., Tomkova, B., & Militky, J. (2024). Effect of Drying Methods on the Thermal and Mechanical Behavior of Bacterial Cellulose Aerogel. *Gels*, *10*(7), Article 7. https://doi.org/10.3390/gels10070474
9. Ciolacu, D. E., & Suflet, D. M. (2018). 11—Cellulose-Based Hydrogels for Medical/Pharmaceutical Applications. In V. Popa & I. Volf (Eds.), *Biomass as Renewable Raw Material to Obtain Bioproducts of High-Tech Value* (pp. 401–439). Elsevier. https://doi.org/10.1016/B978-0-444-63774-1.00011-9
10. Long, L.-Y., Weng, Y.-X., & Wang, Y.-Z. (2018). Cellulose Aerogels: Synthesis, Applications, and Prospects. *Polymers*, *10*(6), Article 6. https://doi.org/10.3390/polym10060623
11. Wei, C., Zhang, Q., Wang, Z., Yang, W., Lu, H., Huang, Z., Yang, W., & Zhu, J. (2023). Recent Advances in MXene-Based Aerogels: Fabrication, Performance and Application. *Advanced Functional Materials*, *33*(9), 2211889. https://doi.org/10.1002/adfm.202211889
12. Revin, V. V., Nazarova, N. B., Tsareva, E. E., Liyaskina, E. V., Revin, V. D., & Pestov, N. A. (2020). Production of Bacterial Cellulose Aerogels With Improved Physico-Mechanical Properties and Antibacterial Effect. *Frontiers in Bioengineering and Biotechnology*, *8*. https://doi.org/10.3389/fbioe.2020.603407
13. Nita, L. E., Ghilan, A., Rusu, A. G., Neamtu, I., & Chiriac, A. P. (2020). New Trends in Bio-Based Aerogels. *Pharmaceutics*, *12*(5), Article 5. https://doi.org/10.3390/pharmaceutics12050449
14. Saleh, A. K., Ray, J. B., El-Sayed, M. H., Alalawy, A. I., Omer, N., Abdelaziz, M. A., & Abouzeid, R. (2024). Functionalization of bacterial cellulose: Exploring diverse applications and biomedical innovations: A review. *International Journal of Biological Macromolecules*, *264*, 130454. https://doi.org/10.1016/j.ijbiomac.2024.130454
15. Nguyen, N. T. T., Nguyen, L. M., Nguyen, T. T. T., Nguyen, D. T. C., & Tran, T. V. (2024). Synthesis strategies, regeneration, cost analysis, challenges and future prospects of bacterial cellulose-based aerogels for water treatment: A review. *Chemosphere*, *362*, 142654. https://doi.org/10.1016/j.chemosphere.2024.142654

16. Al Abdallah, H., Tannous, J. H., & Abu-Jdayil, B. (2024). Cellulose and nanocellulose aerogels, their preparation methods, and potential applications: A review. *Cellulose*, *31*(4), 2001–2029. https://doi.org/10.1007/s10570-024-05743-w
17. Klemm, D., Heublein, B., Fink, H.-P., & Bohn, A. (2005). Cellulose: Fascinating Biopolymer and Sustainable Raw Material. *Angewandte Chemie International Edition*, *44*(22), 3358–3393. https://doi.org/10.1002/anie.200460587
18. Lin, S.-P., Loira Calvar, I., Catchmark, J. M., Liu, J.-R., Demirci, A., & Cheng, K.-C. (2013). Biosynthesis, production and applications of bacterial cellulose. *Cellulose*, *20*(5), 2191–2219. https://doi.org/10.1007/s10570-013-9994-3
19. Jonas, R., & Farah, L. F. (1998). Production and application of microbial cellulose. *Polymer Degradation and Stability, Biodegradable Polymers and Macromolecules*, *59*(1), 101–106. https://doi.org/10.1016/S0141-3910(97)00197-3
20. Catarino, R. P. F., Mascareli, V. A. B., Leite da Costa, V. L., Pavanello, A. C. L., & Spinosa, W. A. (n.d.). Sustainability and Influencing Factors in Bacterial Cellulose Production: A Review of the Impact of Microorganisms, Culture Media and Cultivation Methods. *Food Technology and Biotechnology*, *63*(3), 332–350. https://doi.org/10.17113/ftb.63.03.25.8746
21. Tsouko, E., Pilafidis, S., Kourmentza, K., Gomes, H. I., Sarris, G., Koralli, P., Papagiannopoulos, A., Pispas, S., & Sarris, D. (2024). A sustainable bioprocess to produce bacterial cellulose (BC) using waste streams from wine distilleries and the biodiesel industry: Evaluation of BC for adsorption of phenolic compounds, dyes and metals. *Biotechnology for Biofuels and Bioproducts*, *17*(1), 40. https://doi.org/10.1186/s13068-024-02488-3
22. Hussain, Z., Sajjad, W., Khan, T., & Wahid, F. (2019). Production of bacterial cellulose from industrial wastes: A review. *Cellulose*, *26*(5), 2895–2911. https://doi.org/10.1007/s10570-019-02307-1
23. Abol-Fotouh, D., Hassan, M. A., Shokry, H., Roig, A., Azab, M. S., & Kashyout, A. E.-H. B. (2020). Bacterial nanocellulose from agro-industrial wastes: Low-cost and enhanced production by Komagataeibacter saccharivorans MD1. *Scientific Reports*, *10*(1), 3491. https://doi.org/10.1038/s41598-020-60315-9
24. Revin, V. V., Pestov, N. A., Shchankin, M. V., Mishkin, V. P., Platonov, V. I., & Uglanov, D. A. (2019). A Study of the Physical and Mechanical Properties of Aerogels Obtained from Bacterial Cellulose. *Biomacromolecules*, *20*(3), 1401–1411. https://doi.org/10.1021/acs.biomac.8b01816
25. Fleury, B., Abraham, E., De La Cruz, J. A., Chandrasekar, V. S., Senyuk, B., Liu, Q., Cherpak, V., Park, S., ten Hove, J. B., & Smalyukh, I. I. (2020). Aerogel from Sustainably Grown Bacterial Cellulose Pellicles as a Thermally Insulative Film for Building Envelopes. *ACS Applied Materials & Interfaces*, *12*(30), 34115–34121. https://doi.org/10.1021/acsami.0c08879
26. Baraka, F., Ganesan, K., Milow, B., & Labidi, J. (2024). Cellulose nanofiber aerogels: Effect of the composition and the drying method. *Cellulose*, *31*(16), 9699–9713. https://doi.org/10.1007/s10570-024-06191-2
27. Ruan, J.-Q., Xie, K.-Y., Wan, J.-N., Chen, Q.-Y., Zuo, X., Li, X., Wu, X., Fei, C., & Yao, S. (2024). Effects of Freeze-Drying Processes on the Acoustic Absorption

Performance of Sustainable Cellulose Nanocrystal Aerogels. *Gels*, *10*(2), Article 2. https://doi.org/10.3390/gels10020141
28. Zhang, X., Yu, Y., Jiang, Z., & Wang, H. (2015). The effect of freezing speed and hydrogel concentration on the microstructure and compressive performance of bamboo-based cellulose aerogel. *Journal of Wood Science*, *61*(6), Article 6. https://doi.org/10.1007/s10086-015-1514-7
29. García-González, C. A., Camino-Rey, M. C., Alnaief, M., Zetzl, C., & Smirnova, I. (2012). Supercritical drying of aerogels using CO2: Effect of extraction time on the end material textural properties. *The Journal of Supercritical Fluids, Special Edition on the Occasion of Gerd Brunner's 70th Birthday*, *66*, 297–306. https://doi.org/10.1016/j.supflu.2012.02.026
30. Sözcü, Ş., Wiener, J., Frajová, J., Venkataraman, M., Tomková, B., Kalmár, J., Forgács, A., & Militký, J. (2026). Effect of drying methods on Acetobacter xylinum bacterial cellulose aerogels and cryogels. *Scientific Reports*. https://doi.org/10.1038/s41598-026-42244-1
31. Illa, M. P., Sharma, C. S., & Khandelwal, M. (2019). Tuning the physiochemical properties of bacterial cellulose: Effect of drying conditions. *Journal of Materials Science*, *54*(18), 12024–12035. https://doi.org/10.1007/s10853-019-03737-9
32. Mohamad, S., Abdullah, L. C., Jamari, S. S., Al Edrus, S. S. O., Aung, M. M., & Mohamad, S. F. S. (2022). Influence of drying method on the crystal structure and thermal property of oil palm frond juice-based bacterial cellulose. *Journal of Materials Science*, *57*(2), 1462–1473. https://doi.org/10.1007/s10853-021-06685-5
33. Zeng, M., Laromaine, A., & Roig, A. (2014). Bacterial cellulose films: Influence of bacterial strain and drying route on film properties. *Cellulose*, *21*(6), 4455–4469. https://doi.org/10.1007/s10570-014-0408-y
34. Maryati, Y., Melanie, H., Handayani, W., & Yasman, Y. (2024). Bacterial Cellulose Production from Fermented Fruits and Vegetables Byproducts: A Comprehensive Study on Chemical and Morphological Properties. *Karbala International Journal of Modern Science*, *10*(4). https://doi.org/10.33640/2405-609X.3376
35. Gilmour, K. A., Aljannat, M., Markwell, C., James, P., Scott, J., Jiang, Y., Torun, H., Dade-Robertson, M., & Zhang, M. (2023). Biofilm inspired fabrication of functional bacterial cellulose through ex-situ and in-situ approaches. *Carbohydrate Polymers*, *304*, 120482. https://doi.org/10.1016/j.carbpol.2022.120482
36. Galdino, C. J. S., Maia, A. D., Meira, H. M., Souza, T. C., Amorim, J. D. P., Almeida, F. C. G., Costa, A. F. S., & Sarubbo, L. A. (2020). Use of a bacterial cellulose filter for the removal of oil from wastewater. *Process Biochemistry*, *91*, 288–296. https://doi.org/10.1016/j.procbio.2019.12.020
37. Zhang, X., Zhao, X., Xue, T., Yang, F., Fan, W., & Liu, T. (2020). Bidirectional anisotropic polyimide/bacterial cellulose aerogels by freeze-drying for super-thermal insulation. *Chemical Engineering Journal*, *385*, 123963. https://doi.org/10.1016/j.cej.2019.123963
38. Liebner, F., Haimer, E., Wendland, M., Neouze, M.-A., Schlufter, K., Miethe, P., Heinze, T., Potthast, A., & Rosenau, T. (2010). Aerogels from Unaltered Bacterial Cellulose: Application of scCO 2 Drying for the Preparation of Shaped, Ultra-

Lightweight Cellulosic Aerogels. *Macromolecular Bioscience*, *10*, 349–352. https://doi.org/10.1002/mabi.200900371
39. Sozcu, S., Frajova, J., Wiener, J., Venkataraman, M., Tomkova, B., & Militky, J. (2025). Synthesis of Acetobacter xylinum Bacterial Cellulose Aerogels and Their Effect on the Selected Properties. *Gels*, *11*(4), Article 4. https://doi.org/10.3390/gels11040272
40. Hu, S., Wang, D., Křemenáková, D., & Militký, J. (2023). Washable and breathable ultrathin copper-coated nonwoven polyethylene terephthalate (PET) fabric with chlorinated poly-para-xylylene (parylene-C) encapsulation for electromagnetic interference shielding application. *Textile Research Journal*, *93*(17–18), 3982–3998. https://doi.org/10.1177/00405175231168418
41. ZHANG, X. (2025). *Thermoelectric Behavior of Copper-Nickel Polyethylene Terephthalate Fabric* [Dissertation, Technical University of Liberec, Faculty of Textiles]. Available from: https://theses.cz/id/bi2pex/
42. Lázár, I., & Fábián, I. (2016). A Continuous Extraction and Pumpless Supercritical CO2 Drying System for Laboratory-Scale Aerogel Production. *Gels*, *2*(4), 26. https://doi.org/10.3390/gels2040026
43. Brown, C. A. (2017, October). *Introduction to Surface Roughness Measurement - Olympus Device Roughness measurement guidebook*. Olympus laser scanning microscope -Measuring Laser Microscope -OLS5100 LEXT. https://share.google/l6UJo3gAFdhfAC6q8
44. YL. (2023, October 29). Surface Roughness Parameters: Ra & Rz Calculation [Test Company]. *IPQC-In Process Quality Control*. https://www.ipqcco.com/blog/surface-roughness-parameters-calculation-how-to-determine-calculate-ra-rz
45. Wang, D., Venkataraman, M., Hu, S., Kremenakova, D., & Militky, J. (2025). Corrugated structural effects on the thermal and sound properties of functional nonwoven materials for construction applications. *Discover Materials*. https://doi.org/10.1007/s43939-025-00492-4
46. *DS1923-F5# Hygrochron Temperature and Humidity Data Logger*. (n.d.). iButtonLink. Retrieved March 5, 2026, from https://www.ibuttonlink.com/products/ds1923
47. Eser, M., Emmerich, L., Gurbuz, C., & Marburg, S. (2025). Deep Learning-Assisted Two-Cavity Method for Estimating Sound Propagation Characteristics in Porous Media. *Journal of Theoretical and Computational Acoustics*, *33*(02), 2440001. https://doi.org/10.1142/S2591728524400012
48. Yang, T., Eser, M., Xiong, X., Groby, J.-P., Schmid, J. M., Maeder, M., Chang, Y.-H., & Marburg, S. (2025). Experiment-driven simplification of Johnson-Champoux-Allard-Lafarge model for fibrous materials. *The Journal of the Acoustical Society of America*, *157*(5), 3497–3507. https://doi.org/10.1121/10.0036644
49. Wang, X., Zhang, Y., Jiang, H., Song, Y., Zhou, Z., & Zhao, H. (2016). Fabrication and characterization of nano-cellulose aerogels via supercritical CO2 drying technology. *Materials Letters*, *183*, 179–182. https://doi.org/10.1016/j.matlet.2016.07.081
50. McKenzie, J. S., Jurado, J. M., & de Pablos, F. (2010). Characterisation of tea leaves according to their total mineral content by means of probabilistic neural networks. *Food Chemistry*, *123*(3), 859–864. https://doi.org/10.1016/j.foodchem.2010.05.007

51. Sound Propagation in Cylindrical Tubes and Porous Materials Having Cylindrical Pores. (2009). In *Propagation of Sound in Porous Media* (pp. 45–72). John Wiley & Sons, Ltd. https://doi.org/10.1002/9780470747339.ch4
52. Sound Propagation in Porous Materials Having a Rigid Frame. (2009). In *Propagation of Sound in Porous Media* (pp. 73–109). John Wiley & Sons, Ltd. https://doi.org/10.1002/9780470747339.ch5
53. *ISO 10534-2:1998 Acoustics—Determination of sound absorption coefficient and impedance in impedance tubes—Part 2: Transfer-function method*. (n.d.). ISO. Retrieved February 23, 2026, from https://www.iso.org/standard/22851.html

9. List of Journal publications by author

Publications in Journal

[1] **Sözcü, Ş.**, Wiener, J., Frajová, J. *et al.* Effect of drying methods on *Acetobacter xylinum* bacterial cellulose aerogels and cryogels. *Sci Rep* (2026). https://doi.org/10.1038/s41598-026-42244-1.

[2] **Sozcu, S.**; Frajova, J.; Wiener, J.; Venkataraman, M.; Tomkova, B.; Militky, J. Effect of Drying Methods on the Thermal and Mechanical Behavior of Bacterial Cellulose Aerogel. Gels 2024, 10, 474. https://doi.org/10.3390/gels10070474.

[3] **Sozcu, S.**; Venkataraman, M.; Wiener, J.; Tomkova, B.; Militky, J.; Mahmood, A. Incorporation of Cellulose-Based Aerogels into Textile Structures. Materials 2024, 17, 27. https://doi.org/10.3390/ma17010027.

[4] **Sozcu, S**.; Frajova, J.; Wiener, J.; Venkataraman, M.; Tomkova, B.; Militky, J. Synthesis of Acetobacter xylinum Bacterial Cellulose Aerogels and Their Effect on the Selected Properties. Gels 2025, 11, 272. https://doi.org/10.3390/gels11040272.

[5] **Sözcü, Ş**.; Wiener, J.; Venkataraman, M.; Tomkova, B.; Yang, T.;, A.; Militky, J. Thermal and Acoustic Behavior of Bacterial Cellulose Aerogels and Cryogels. Discover Materials 2026 (In preparation)

Journal article: Co-author

[1] Venkataraman, M.; **Sözcü, S.**; Militký, J. Radiative Heat Transfer Properties of Fiber–Aerogel Composites for Thermal Insulation. Gels 2025, 11, 538. https://doi.org/10.3390/gels11070538

[2] K. Yang, X. Zhang, M. Venkataraman, J. Wiener, S. Palanisamy, **S. Sozcu**, X. Tan, D. Kremenakova, G. Zhu, J. Yao, J. Militky, Structural Analysis of Phase Change Materials (PCMs)/Expanded Graphite (EG) Composites and Their Thermal Behavior under Hot and Humid Conditions, ChemPlusChem 88 (2023) e202300081. https://doi.org/10.1002/cplu.202300081.

[3] Mahmood, A.; Noman, M.T.; Pechočiaková, M.; Amor, N.; Petrů, M.; Abdelkader, M.; Militký, J.; **Sozcu, S.;** Hassan, S.Z.U. Geopolymers and Fiber-Reinforced

Concrete Composites in Civil Engineering. Polymers 2021, 13, 2099. https://doi.org/10.3390/polym13132099

Contribution in conference proceedings

[1] **Sozcu, S.**; Wiener, J.; Venkataraman, M.; Tomkova, B., and Militky, J. Perspective Way for Sustainability: Bacterial Cellulose Aerogels. Colloquium: RUN-EU Circular Society Event, Netherland, 18-20 February 2026.

[2] **Sozcu, S.**; Wiener, J.; Frajova, J.; Venkataraman, M.; Tomkova, B., and Militky, J. Bacterial Cellulose Aerogels from Acetobacter xylinum: Effects on Different Properties. Queen Mary's College(autonomous), International Conference, Chennai – 600 004, 24-25 July 2025.

[3] **Sozcu, S.**, Venkataraman, M., Wiener, J., Tomkova, T., Mility, J., and Mahmood, A. SYNTHESIS OF CELLULOSE AEROGEL AND THEIR APPLICATION IN THE FIBROUS STRUCTURES, Autex 2024, Conference Liberec.

[4] **Sozcu, S.**; Frajova, J.; Wiener, J.; Venkataraman, M.; Tomkova, B., and Militky, J. CELLULOSE AEROGEL IN TEXTILE COMPOSITE STRUCTURE, Strutex 2024, Conference Liberec.

Book chapters

[1] **Sozcu, S.,** Venkataraman, M., Tomková, B., Militký, J. (2025). Biodegradability and Environmental Impact of Bacterial Cellulose. In: Militký, J., Venkataraman, M. (eds) Fibrous Structures for Sustainable Future. Engineering Materials. Springer, Singapore**.** https://doi.org/10.1007/978-981-95-1382-6_9

[2] **Sozcu, S.,** Venkataraman, M., Tomková, B., Militký, J. (2022). *Cellulose-Based Aerogels Understanding Their Origin, Preparation and Multifunctional Effect of Potential Application.* Selected Topics in Fibrous Materials Science, 2022-09-05. https://dspace.tul.cz/handle/15240/166004 (in TUL printed publication)

[3] Gul, A.; Gallus, I,; **Sozcu, S.**; Yalcinkaya, F. Electrospun Nanofibrous Materials for Oil/Water Separation. American Chemical Society 2022, Oil–Water Mixtures and Emulsions, Volume 1: Membrane Materials for Separation and Treatment. DOI:10.1021/bk-2022-1407.ch002

Quotation

According to Scopus, Sözcü, S. has 174 citations from 9 documents with an h-index of 5 (Author ID: 57342897100).

10. Brief characteristics of previous professional, research and scientific activities

Doctoral Studies

Exams	• Structure and Properties of Textile Fibre 25.02.21 • Theoretical Textile Metrology 11.05.21 • Heat and Mass Transfer in Porous Media 08.03.22 • Macromolecular Chemistry 28.03.23 • Experimental Technique of The Textile 08.12.23
SDE	Comprehensive Doctoral Exam 29.11.24
Teaching Activities	Assisting of Erasmus exchange students during semester and summer periods (2025–2026)
Research projects	• Enhanced Side Luminous Property of Polymer Optical Fiber Incorporated Woven PET Fabrics By using Acetone/Methanol (SGS-2023-6353), project member. • Structural analysis of polyethylene glycol embedding in expanded graphite under different relative humidity (SGS2022-6065), project member. • Effect of geometry and concentration of fly ash and laponite on impact and dynamic mechanical properties of filled epoxy matrix (SGS 2021 -6025)
Other Academic & Service Activities	Contribution to conference organization and on-site support, AUTEX 2024 Conference, Liberec

11. Curriculum Vitae

Şebnem Sözcü| Ph.D. student
Faculty of Textile Engineering
Technical University of Liberec
Mobile: +420 603 268 959
Email: sebnem.szc@gmail.com; sebnem.sozcu@tul.cz

Education

10/2020 – Present
Doctor of Philosophy (Ph.D.), Technical University of Liberec, Liberec, CZ
Textile Faculty, Material Engineering Department
Research Topic: Advanced Fibrous Structures Based on Bacterial Cellulose

09/2016 – 07/2019
Master of Science (M.Sc.), Gaziantep University, Gaziantep, TR
Institute of Science and Technology, Textile Engineering Department, Textile Science and Engineering
Research Topic: The Production of BCF Yarn and Machine Carpet from Recycled Polypropylene Pellets

09/2010 — 06/2015
Bachelor Science, Gaziantep University, Gaziantep, TR
Engineering Faculty, Textile Engineering Department

Internship Experience

Synthesis of Aerogel via Polymeric and Textile Fibers with Sc CO_2 Drying: 06/2023-08/2023
Department of Inorganic and Analytical Chemistry, University of Debrecen, Hungary

Acoustic Absorption Measurement on BC Aerogel sample: 06/2025
TUM School of Engineering and Design, Department of Engineering Physics and Computation, Technical University of Munich, Germany

Professional experience

06/2025- Present
Internal Compliance Specialist – HH Global– Liberec, Czech Republic

08/2023 – 04/2025
Import Trade Compliance Analyst - HONEYWELL INT SRO – Prague, Czech Republic

05/2022 — 03/2023
Import Trade Compliance Analyst - HONEYWELL SPOL SRO- Prague, Czech Republic

03/2020 — 01/2021

Import & Export Supervisor - ASELPLAST AMBALAJ VE TEKSTİL SAN. TİC.A.Ş. - Gaziantep, Turkiye

01/2018 –04/2019
Innovation and Process Specialist/ R&D - Sanat Hali & Kartal Carpet -Gaziantep, Turkiye

06/2016- 12/2017
Customer Representative - Selçuk İplik & Kara Holding - Gaziantep, Turkiye

Language Skills

English (Professional, B2), **Czech** (Elementary, A2), **Turkish** (Native)

12. Recommendation of the supervisor

FACULTY OF TEXTILE ENGINEERING TUL

OPINION OF THE SUPERVISOR ON PH.D. THESIS

THESIS TITLE: Advanced Fibrous Structure Based On Bacterial Cellulose

AUTHOR: Sebnem Sözcü, M.Sc.

The main specific goal of PhD candidate was research and development of a sustainable and additive-free approach for producing bacterial cellulose (BC) aerogels and cryogels from Acetobacter xylinum under standardized cultivation using bio-based feed-stocks, including fermentation by-products. The topic of presented dissertation is undoubtedly up-to-date and it respects innovative current and future trends, which prefer development and manufacturing of new products using biodegradable, environmental friendly materials.

Author has prepared comprehensive study on the effect of drying pathways and pre-freezing strategies on multiscale structure and functional performance (thermal, acoustic, mechanical) of BC materials. Besides large volume of experimental data which confirm the direct influence of the drying processes on the structural and material parameters of final BC aerogels, she also highlights limitations of controlled production conditions resulting from inherent biological variability that influences fibril formation and network architecture.

The thesis as such represents an exhaustive source of information on BC structures with an overlap into many sectors where there is a great interest in these materials (energy sector, chemistry, food industry and many others). In conclusion, there are briefly presented application potential and outlined options of future work.

Finally, it must be said that Sebnem has worked all the time very independently, it was always apparent that she has got a clear idea of what she wants to do and why. Consultations always took the form of an expert discussion showing readiness of PhD student for independent scientific work. After all, this is evident from her publication activities.

Hence, I state the dissertation meets the requirements for the award of the Ph.D. degree, and I recommend it for the defence.

In Liberec, 24.8. 2026

Ing. Blanka Tomková, Ph.D.
Supervisor

Ing. Blanka Tomková, Ph.D. | Assistant Professor | +420 485 536 457 | blanka.tomkova@tul.cz
Technical University of Liberec | Faculty of Textile Engineering | Department of Material Engineering
Studentská 1402/2, 461 17 Liberec 1, Czech Republic | www.ft.tul.cz

13. Reviews of the opponents

OPPONENT OPINION of the dissertation **of the author Sebnem Sözcü, M.Sc.**

„Advanced Fibrous Structures Based on Bacterial Cellulose"

Faculty of Textile Engeneering TU Liberec, 2026

a) *Evaluation of the importance of the dissertation for the field:*

Despite the current geopolitical situation, which partially limits the purchasing power of the population, the consumption of fibre raw materials is still increasing. This is also due to the fact that fibrous materials are finding new applications. Covering this increase with petrochemical-based synthetic fibers cannot be considered sustainable; But even the intensive production of classic natural cellulose fibres – especially cotton, leaves negative environmental consequences due to the high consumption of water and the necessary pesticides – during cultivation, but also during processing and maintenance processes, during which water is often contaminated with hazardous chemicals. In response, more and more attention is being paid to the development of materials and composites based on bio-production. Supported by the priorities of the bioeconomy, the transfer of these new materials to industrial applications is also developing. Bacterial cellulose is undoubtedly one of such materials. In an effort to find new applications for this bio-material, which would reduce the complexity of purification procedures (removal of lignin, hemicelluloses and pectins) necessary especially for medical applications, the author combined the study of its use with another form of emerging materials – aerogels. They can also use a cellulose-based biopolymer as a starting precursor. This combines the sustainability of cellulose with the structural advantages of aerogels. Cellulose aerogels are prepared in two stages – after the formation of the sol-gel form, their porous structure is stabilized by drying. This is due to the fact that minor deviations in the biological activity during which bacterial cellulose is produced, as well as the subsequent finalization conditions – alternative drying procedures were monitored – in air at room temperature, in supercritical CO2 (ScCO2) and under various freeze-drying conditions.

The thesis brings a summary of an extensive evaluation of the consequences of the selected finalization procedures, especially the alternatives of freeze-drying (lyophilization) on the resulting structures and thus the final functional - thermal insulation and filtration capabilities of bio-cellulose aerogels (cryogels). The benefit of the detailed study is therefore mainly the comparison of their thermal and acoustic insulation capabilities achieved by various drying procedures. The next part of the evaluation also focused on the possibility of reusing regenerated bacterial cellulose.

b) *Statement on the procedure for solving the problem, the methods used and the fulfilment of the set goal:*

The presented work proves that the author carried out a very extensive literature search in the initial phase, which could be used for the chosen procedure of the study itself (104 references). However, the professional level of the work is also evidenced by an overview of

published works in which the aspirant is either the main author (5) or co-author (3), as well as chapters of published books (3). The aspirant's activity at professional conferences(4) is also documented – in all cases, these are papers with good creditworthiness. The goal of the dissertation was fulfilled.

c) *Results of the dissertation and the significance of the author's original contribution:*

Also with regard to the fact that the search for the possibilities of using emerging "bio-based" materials is part of the long-term strategy for the sustainable development of the (European) textile industry, the focus and the new results achieved supporting the possibility of new applications of bio-cellulose in the form of functional aero/cryogels can be evaluated as a contribution to the implementation of this strategy. An overview of the results of extensive evaluations is processed, which provide new information for the future expansion of these bio-materials in the field of insulation – thermal and acoustic, conditioned – as the results prove by the methods of final drying. Aerogel forms themselves are among the emerging materials.

d) Oher opinion:

The author's systematic work is remarkable, as well as the processing of a wide range of results and their evaluation. The thesis is thus clear even with a considerable scope and allows for a good orientation in its content. The language level is very good, the thesis is prepared in English, which the doctoral student obviously has a perfect command of.

e) Statement on the publications of the doctoral student:

Already in part b) I used extensive publishing and presentation activities (professional conferences) as one of the tools for a very comprehensive and careful presentation of the work performed. This proves that the doctoral student is aware of the importance of presenting the results as part of supporting the path of experimental activities to industrial implementations. It is also important for the development of the necessary multidisciplinary solutions, which are indispensable today.

f)Final statement of the opponent:

In view of the above

I recommend the dissertation of the author Sebnem Sözcü, M.Sc. for defense.

Ing. Jan Marek, CSc. – oponent

Ve Dvoře Králové n.Lab. 29.06.2026

Opponent's Review of the Dissertation
"Advanced Fibrous Structures Based on Bacterial Cellulose"
submitted by Sebnem Sözcü, M.Sc.
(Study programme: P0723D270003 Textile Engineering)

The potential applications of bacterial cellulose have not yet been fully exploited. It is a biomaterial with enormous potential, distinguished by its purity, water-retention capacity, and high mechanical strength. From this perspective, the dissertation makes a significant contribution, as it provides new insights into the effect of the drying process on the structure and surface parameters of the prepared bacterial cellulose. The findings can be applied in a wide range of fields; the author highlights its use in thermal insulation and filtration processes, but the findings may also be beneficial in other fields.

To achieve the objectives of the dissertation, the author used an original method for preparing the test samples based on sweetened black tea and the bacterium *Komagataeibacter xylinus* (formerly *Acetobacter xylinum*). This fermentation process has been known for more than 2,000 years. In this case, BC is a byproduct formed on the surface during the preparation of fermented beverages. Static cultivation was performed at a temperature of 24°C. Subsequently, the resulting pellicles were mechanically disintegrated and freeze-dried. The BC prepared in this manner was used as a standard for the further investigation of the effects of drying and freezing on the structural changes and surface properties of BC aerogels and cryogels.

The author logically outlined the research approach and defined six interconnected main goals, which formed the conceptual framework of the dissertation. Her research was based on 17 defined types of samples prepared using several methods described in the dissertation. A wide range of methods was used to characterize the samples; these methods are properly defined in the dissertation, and the results are well presented. The objectives of the dissertation were successfully achieved.

The results of the dissertation have considerable informational value, based on a large volume of experimental data on drying processes and their effect on the structure of BC, as well as on other key parameters such as surface geometry or the arrangement of nanofibrillar segments. The author's original contributions include the sections demonstrating the critical influence of drying on the stability of BC's open pores. This finding opens up further possibilities for the use of stabilized open structures in the energy sector, catalytic processes, and the functionalization of advanced composites, etc. In Section 6.4, the author briefly addresses the functionalization of regenerated bacterial cellulose with crystalline graphite, which is just one of many potential directions for future research.

The dissertation is systematically organized and follows a standard structure, providing all the required information. The initial step of the dissertation is the preparation of samples under defined conditions, including room-temperature drying, freezing, lyophilization, and drying without fabric support. This is followed by eight test series, a description of the results, and a discussion. The conclusion of the dissertation states that drying processes are crucial for the structural and functional performance of bacterial cellulose.

The formatting meets the required standards; the text is supplemented by 49 figures and 12 tables. The dissertation is comprehensible throughout and is written in English with a Czech abstract.

Regarding the author's publication activity, she submitted five scholarly articles as the first author and is listed as a co-author on three additional articles. She also presented four conference papers and published three chapters in scholarly books. The number of publications is well above average. The publications are of high quality and are widely cited in the Web of Science database.

As part of the dissertation defence, the candidate should answer the following questions:

1. Research shows that BC production could have a much larger market share than it currently does. What are the reasons for the difficulty in establishing BC on the market?

2. In which application areas do you expect the greatest growth in the future?

In conclusion, the dissertation entitled "Advanced Fibrous Structures Based on Bacterial Cellulose" by Sebnem Sözcü, M.Sc. meets the requirements for the award of the Ph.D. degree. Therefore, **I recommend** that it be accepted for defence.

In Zlín, 29 June 2026

prof. Ing. Petr Sáha, CSc., dr.h.c
University Institute
Tomas Bata University in Zlín